UNIVERSITY OF SEVILLE
POLYTECHNIC UNIVERSITY OF CATALONIA

BRIKEN measurements of half-lives for Ce to Nd nuclei relevant for the formation of the r-process rare-earth peak (A∼160).

MASTERS' DEGREE IN NUCLEAR PHYSICS
FINAL MASTERS' PROJECT

by
Araceli Navarro Fernández

Supervisors:
Dr. Ariel Tarifeño Saldivia UPC, Barcelona
Dr. José M. Arias Carrasco US, Sevilla

July 2019

Abstract

The Rare Earth Peak (REP) is a small, but clearly distinctive, peak around mass A 160 in the elemental solar system abundances created by the rapid neutron-capture process (r-process). Understanding the REP formation offers a unique probe for the study of the late times environmental conditions in the r-process site. According to theoretical models, half-lives ($T_{1/2}$) and beta-delayed neutron emission probabilities (P_n) play an important role on the formation of the REP.

In order to be able to measure this parameters, advanced instrumentation has been carefully developed. The largest and most efficient -delayed neutron detector of its kind has been built by the BRIKEN collaboration, at RIKEN Nishina Center. The BRIKEN project, launched in 2016 at RIBF in the RIKEN Nishina Center, aims to measure the decay properties (primarily $T_{1/2}$ and P_n values) for a large number of isotopes on the path of the r-process, by using the BRIKEN neutron detector (the world largest beta-delayed counter), the AIDA implantation detector and two CLOVER-type HPGe detectors. The last run of this experiment was performed in 2018 with a setting centered on 165Pm. This project focuses on the preliminary data analysis of the NP1612-RIBF148 experiment, that took place on October 2018 at RIKEN, Nishina center. The main objective of this preliminary analysis was the obtention of experimental values for the half-lives of nuclei from Ce to Nd. For that, a C++ software program was implemented. The results obtained are compared with measurements by the EURICA's collaboration. The half-lives obtained for this report seem to be in agreement with the currently available experimental values, obtained by EURICA's collaboration in 2017. Considerable reduction of the half-lives uncertainties has been achieved.

This report has been divided in six Sections + one Appendix. The first section (Section 1) aims to explain the motivation behind accurate experimental measurements of nuclear properties. This section focuses on the importance accurate measurements of $T_{1/2}$ and P_n values have on the description of the r-process. For that, concepts such as r-process, β-decay, *beta*-decay neutron emission and REP will be introduced. Details about the current status of the available experimental data of nuclear properties of nuclei relevant for the REP region will be also introduced in this first section, along with an introduction to the BRIKEN collaboration and it's contribution to the experimental measurements of these properties.

Section 2 presents an overall introduction to the experimental set up used by BRIKEN's collaboration, including a description of the three main detection systems, BigRIPS, AIDA and BRIKEN. This section also includes a brief description of the data's structure. For the preliminary data analysis a software program was implemented. Section 3 describes the data analysis systematics and the basic formalism behind this software program. A more detailed description of the program itself and its usage can be found in Appendix A. This program was detailedly tested before proceeding to the real data analysis. Section 4 presents the most relevant features found whilst testing this program with artificially generated data. This section studies features such as the effects background sources and statistical fluctuations have in the accuracy of the results. Finally, Section 5 presents the results obtained for the half lives of the isotopes $^{15-158}Cd$, $^{155-160}Pr$ and $^{157-162}Nd$, alongside a comparison with previously measured ones.

Table of Contents

List of Figures

List of Tables

1. Introduction.

This first section aims to explain why accurate experimental measurements of nuclear properties, such as half-lives, are crucial for understanding the formation processes of the elements in the universe. In order to do that, a small introduction about elemental nucleosynthesis will be given in subsection 1.1. It will be followed by an explanation about the most common decay methods of neutron rich nuclei (β-decay and β-delayed neutron emission) in subsection 1.2, this is crucial to understand the solar abundance pattern of stable elements.

The nuclei under study in this project have mass numbers around A $\sim$ 160. Subsection 1.3 clarifies why this specific nuclei are under study by introducing the concept of REP peak. Subsection 1.4 justifies the importance nuclear properties have in the REP peak formation. This first section finishes with an overview of the currently available experimental data of nuclear properties for nuclei in the REP region (Subsection 1.5), and gives an insight into the contribution of the BRIKEN collaboration in measurements of nuclear properties (Subsection 1.6).

1.1. Elemental Nucleosynthesis.

The origin of the elements in the universe is a mystery that has fascinated physicists for many decades. It was around 1920s when Arthur Eddington proposed for the first time that stars obtained their energy from nuclear fusion of hydrogen to helium and also raised the possibility that heavier elements were produced in stars [1]. This was the first step towards the idea of stellar nucleosynthesis. In 1957, the B2FH paper was published [2]. This lengthy paper provided the road map to how the most abundant elements on Earth had been synthesized within stars from their initial hydrogen and helium. The paper even comprehensively outlined and analyzed several key processes that are responsible for the nucleosynthesis of elements heavier than iron.

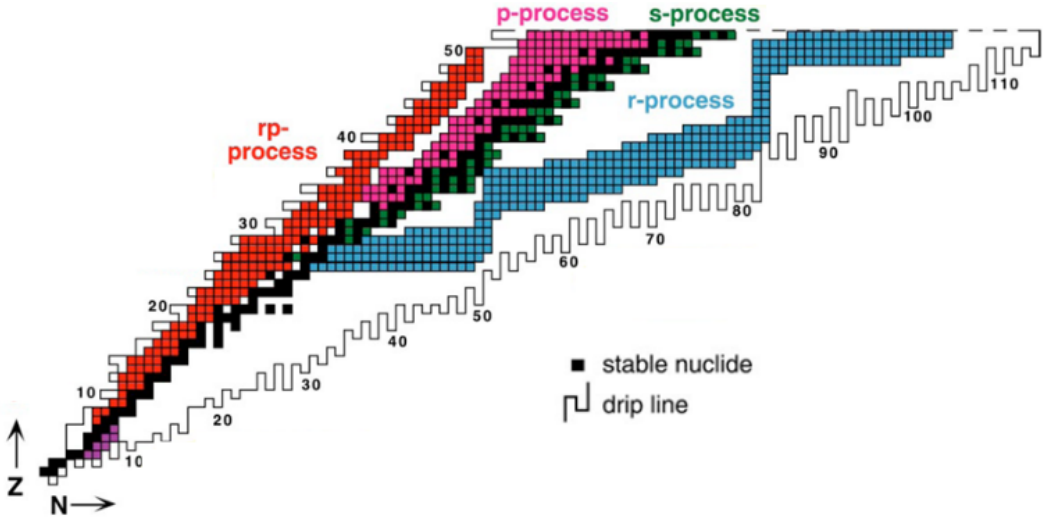

Figure 1: Chart of nuclides and most relevant formation processes. From [3].

Since the B2FH paper, elements were mainly classified as p-process, s-process or r-process elements, depending on their formation mechanism. The p-process refers to the proton capture process and it is responsible of the production of proton rich isotopes [4]. The s-process and the r-process are neutron capture processes, and are the major contributors to the abundances of stable elements. Depending on the available neutron densities the neutron captures can occur slowly (s-process) or rapidly (r-process). In figure 1, a color coded chart of nuclei has been represented. Different colors indicate different formation processes.

1.1.1 The s-process

The s-process accounts for half of the heavy nuclei in the solar system, and it stands for slow neutron capture process. In this case, a nucleus catches a neutron and becomes an isotope with one higher atomic mass. This neutron capture processes is slow in the sense that the new formed nuclei has time to decay to an stable nucleus before another neutron is captured. The s-process is believed to occur over time scales of thousands of years, passing decades between neutron captures. The s-process is believed to take place mostly in asymptotic giant branch stars [5].

1.1.2. The r-process

The r-process entails a succession of rapid neutron captures, typically beginning with nuclei around the ^{56}Fe peak. The captures must be rapid in the sense that the time scale of a successive neutron capture (τ_n) of an unstable isotope is shorter than the one of its radioactive decay (β-decay, τ_β) [6] . This sequence is halted only when the increasingly neutron-rich nuclei cannot physically retain another neutron and become unstable to spontaneous fission. Hence the r-process path reaches very neutron-rich isotopes which subsequently decay back to the valley of stability.

This process is believed to occur over time scales of seconds in explosive environments. The formation site for the r-process is something that has been under debate for many years. It was clear that it had to be an environment with a very high neutron rich flux. Theoretical models were predicting type two super novas and neutron star mergers to be the sites for the r-process to occur [7].

1.2 β-Decay and Neutron Emission Probability.

Most of the nuclei formed by capture processes are going to be unstable to radioactive decay. So after it's formation by either the s or r-processes these elements will decay until stability. In the neutron rich part of the nuclei chart, β^- decay and β^- delayed neutron emission are going to be the most common decay methods. In a nucleus, β^- decay changes both Z and N: by one unit: Z $\rightarrow$ Z + 1, N $\rightarrow$ N - 1, so that A = Z + N remains constant [8]. The generic equation for β^- emission is:

$$ {}^{A}_{Z}X_1 = {}^{A}_{Z+1}X_2 + e^- + v_e^- \tag{1} $$

Where A and Z are the mass number and atomic number of the decaying nucleus, and X_1 and X_2 are the initial and final elements, respectively. e^- is the emitted electron and v_e^-

is an electron anti-neutrino. To clarify the notation, in the following discussion whenever β decay is mentioned, we are referring to β^- decay.

The parent nuclei can decay to different states of the daughter nuclei, it can be either to the ground state or to an excited state. Due to the nature of the nuclei under analysis, it will be energetically possible that a fast neutrons are emitted following the β-decay. This process is known as β delayed neutron emission. A schematic illustration of this process is represented by Figure 2. The equation for such β_n emission is:

$$ {}^{A}_{Z}X_1 = {}^{A-1}_{Z+1}X_5 + n + e^- + v_e^- \tag{2} $$

The probability of emitting a neutron after β-decay is sometimes referred as the P_n value. It is also possible in some cases to emit more than one neutron after a β-decay. The probability of those events to happen is referred to as P_{2n}, P_{3n}, P_{4n}, etc. depending on the number of neutrons emitted. These values will be nuclei dependent, and they are critical for understanding the decay path of neutron rich nuclei towards stability.

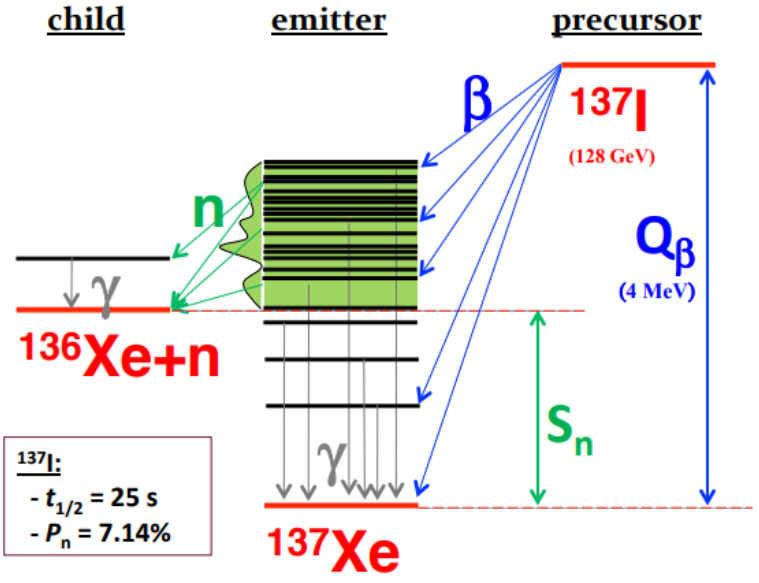

Figure 2: Illustration of β^- and β_n^- decay processes from the parent nucleus (^{137}I). Several states can be fed via β-decay. In green, states with energies higher than the neutron separation energy. From [9].

1.3 Solar System composition, REP peak.

The isotopic composition of the elements in the solar system has served as an important source of information for nucleosynthesis concepts [5]. Much effort has been devoted over the years to obtain a precise measurement of the solar system abundances [6]. In figure 3, a graph of solar abundances, for heavy elements, is displayed on a logarithmic scale. In this figure, nuclei have been separated depending on their formation process. It is clear from figure 3 that the r-process and the s-process are the main contributors to the total abundance of stable elements. Decomposing the isotopic abundance in the different formation processes

is not as easy as it might be thought, and to some extent, it depends on the models of heavy nuclei synthesis. The formation sites and parameters needed to describe the s-process are well known, and the models describing this process are believed to be accurate. The r-process is a different story. The contribution of the r-process for each isotope is obtained by subtracting the s-process contribution from the observed solar abundances.

By doing so, predominant r-process peaks appear at A $\sim$ 130, 160, 195. In particular, the abundances of the rare earth elements, the peak at A $\sim$ 160, are some of the most precisely known in the solar system. This peak is known as the REP (Rare Earth Peak), red circle in figure 3. Studying the rare earth elements and the associated peak is an ideal choice for properly exploring and understanding the particularities of the rapid neutron capture process.

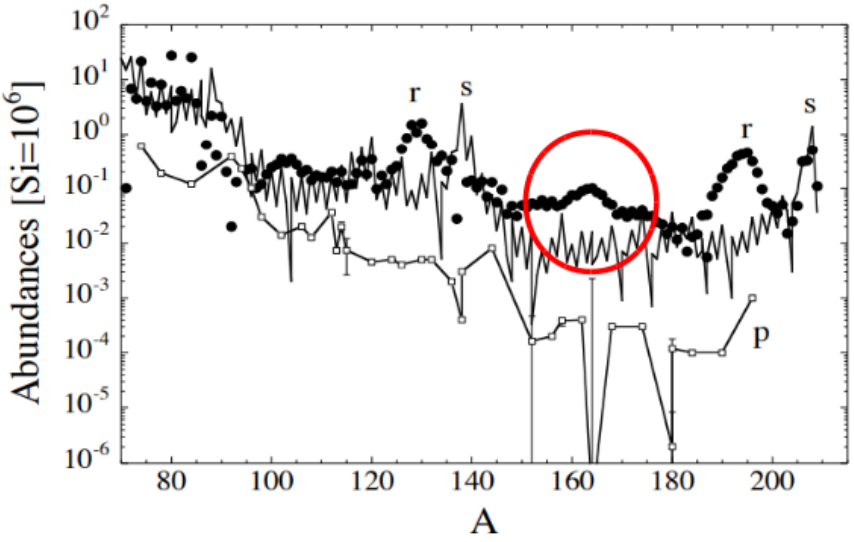

Figure 3: Solar abundances of heavy nuclei. s-process, solid line. r-process, dots. p-process, squares. Vertical lines are possible uncertainties. The solid red circle indicates the REP peak. From [6]

1.4 Impact of nuclear properties on r-process nucleosynthesis and REP peak formation.

To properly describe the r-process and the subsequent elemental abundances, a detailed description of both the neutron rich nuclei formation and it's decay towards stability is necessary. Essential parameters for this description involve the neutron flux, which deeply depends on the formation site, and nuclear properties of nuclei involved in the process, such as masses, β-decays and neutron emission rates. Close to stability, experimental values of this nuclear properties are available. Nevertheless, as we move to nuclei further away from stability experimental measurements of these quantities become highly inaccurate or nonexistent.

For a theoretical determination of this properties an inverse process is commonly used [10]. As aforementioned, the contribution of the r-process for each isotope is obtained by subtracting the s-process contribution from the observed solar abundances. Nuclear properties

can then be calculated by Monte Carlo simulations that try to match of the r-process network output to the observed abundances. Figure 4 show how different theoretical approaches produce markedly different predictions [11].

Small variations in the values of this properties deeply affect the overall r-process abundance pattern. M.R. Munpower, et. al. studied in detail the effect of this individual nuclear properties on r-process nucleosynthesis models [11] [10]. Figure 5 shows the effect uncertainties in half-life values have when calculating r-process abundances with the FRDM1995 [12] model. This big fluctuations are a common feature of all theoretical models as shown in [11].

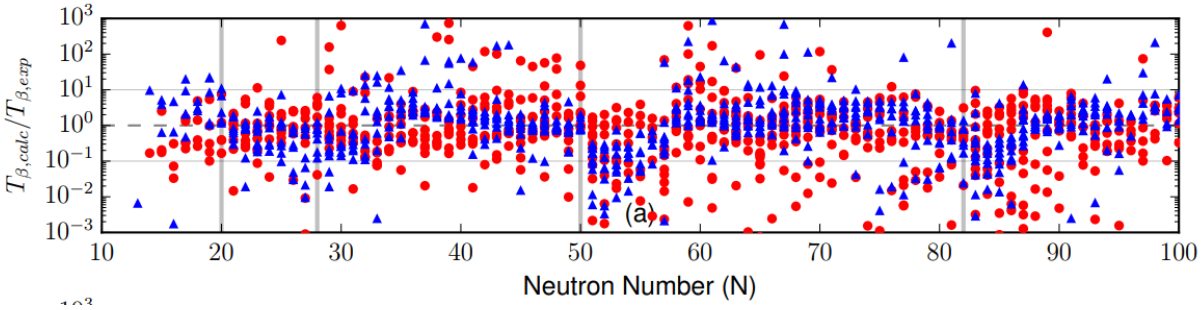

Figure 4: Comparison of theoretical β-decay half lives to experimentally measured values from NNDC database [14]versus neutron number. Red circles, FRDM1995 + QRPA data points [12]. Blue triangles, KTUY05 + gross theory data points [13]. Graph from [11]

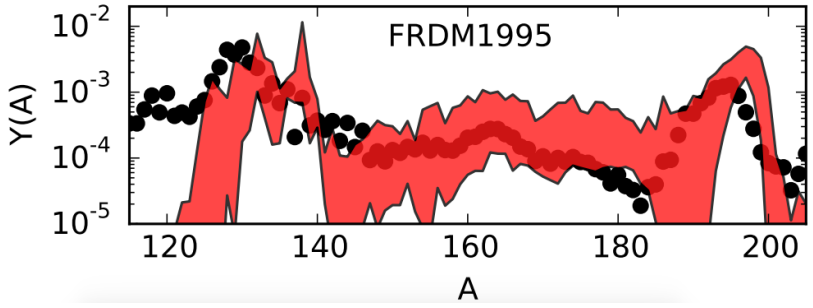

Figure 5: Variance in isotopic abundance pattern from uncertain β-decay half-lives. Theoretial model FRDM1995 [12]. Graph from [11].

Inaccuracies in the prediction of solar system abundances and considerable discrepancies between the different theoretical models, arises the necessity to obtain precise experimental measurements of nuclear properties for nuclei involved in the r-process formation path. Big efforts and resources are being invested into the production of exotic neutron rich nuclei as well as accurate measurements of their properties. In the following two subsections a brief summary of the current status of the available experimental nuclear properties for the REP region will be given.

1.5 Status of experimental nuclear properties in REP region.

For this project, especial attention is going to be placed on experimental measurements of the half-lives. No details about mass measurements are going to be given, but information about mass measurements can be found in [15]. No experimental values for neutron emission probabilities of nuclei in this region are available at the moment. NP1612RIBF148 allowed to experimentally measure such neutron emission probabilities for the very first time. A detailed data analysis of the experiment is on going and experimental P_n values for this nuclei will be available in a near future. The present document focuses only in the experimental half-life calculation so no detailed description of P_n value calculation from experimental data will be given.

The current available experimental values of half-lives of nuclei involved in the REP peak formation, were measured by EURICA's collaboration at RIKEN, Nishina Center. The experiment was a β-decay spectroscopy experiment optimized for transmission of ^{158}Nd and ^{170}Dy. Detailed information about the experimental set up used by EURICA's collaboration can be found in [16]. This collaboration managed to obtain 98 β-decay half lives of neutron rich nuclei from $_{55}$Cs to $_{67}Ho$. In figure 6 a close up of the region of interest for the REP peak formation, according to [17], can be found. Nuclei enclosed by the green and pink lines were to some extent measured by EURICA's collaboration. Half-lives of nuclei beyond the pink line had never been experimentally measured before BRIKEN's experiment.

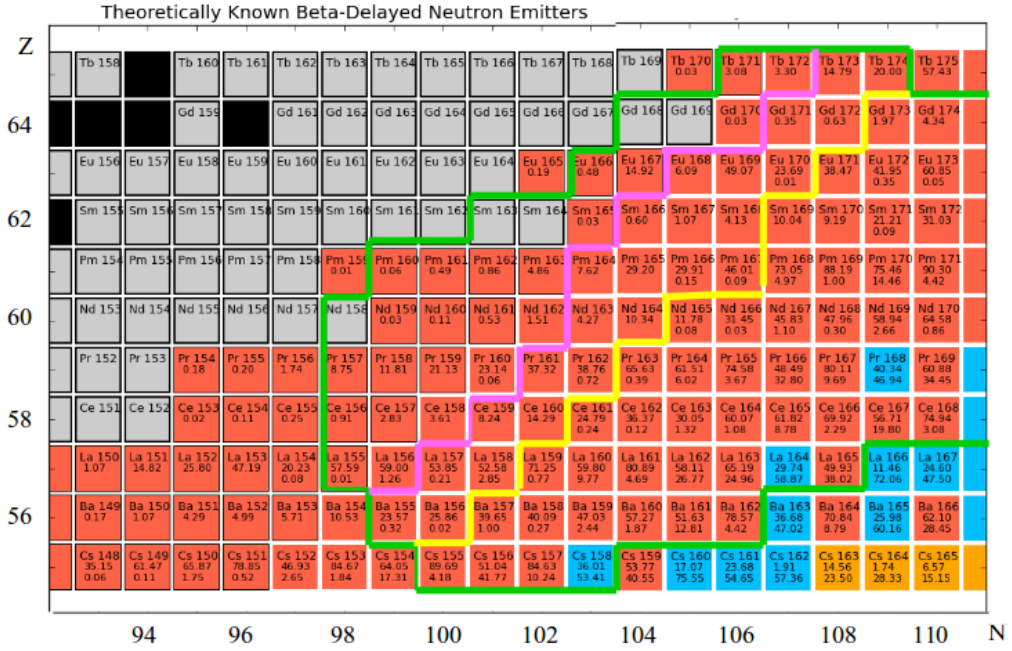

Figure 6: Green enclosure, nuclei relevant for understanding REP peak formation. Pink line, limits of EURICA's experimental campaign. Yellow line, limits of BRIKEN's experimental campaign. The different cell colors are related to neutron emission probabilities. Grey, no neutron emission expected. Red, one neutron emission expected. Blue, two neutron emission dominates. Orange, three neutron emission dominates. The numbers in each cell correspond to the P_n values predicted by Möller in 2003. Figure taken from [18]

A summary of the results obtained by EURICA's campaign have been summarized in figure 7. This results were compared to some of the most relevant theoretical models. Figure 7 clearly shows the systematic trends of the half lives of the nuclei in this region as well as the theoretical models discrepancies, both between themselves and also with the experimental values.

1.6. The BRIKEN Project. NP1612RIBF148 Experiment Overview.

The BRIKEN project [25] was launched in 2016 at RIKEN Nishina Center [26]. Right now, the BRIKEN collaboration comprises 20 research institutions and more than 50 scientists. This collaboration aims to measure the decay properties, primarily $T_{1/2}$ and P_n values, for a large number of nuclei. Six experimental proposals have been approved, and they approximately cover the hole path of the r-process. Figure 8 shows the areas covered by each one of this campaigns. The red numbers in this figure is what it is expected to be obtained from this campaigns. If the predictions are accurate, a total of 235 new P_{1n} values, 90 new P_{2n} values, 17 new P_{3n} values, 5 new P_{4n} and 115 new half-lives will be obtained.

In particular, NP1612RIBF148 experiment aims to measure the nuclear properties of nuclei involved in the REP peak formation. The yellow line in figure 7 delimits the area of nuclei for which have-lives calculation was possible at BRIKEN's campaign. From figure 7 one can already observe that BRIKEN's setting was slightly more exotic than EURICA's setting.

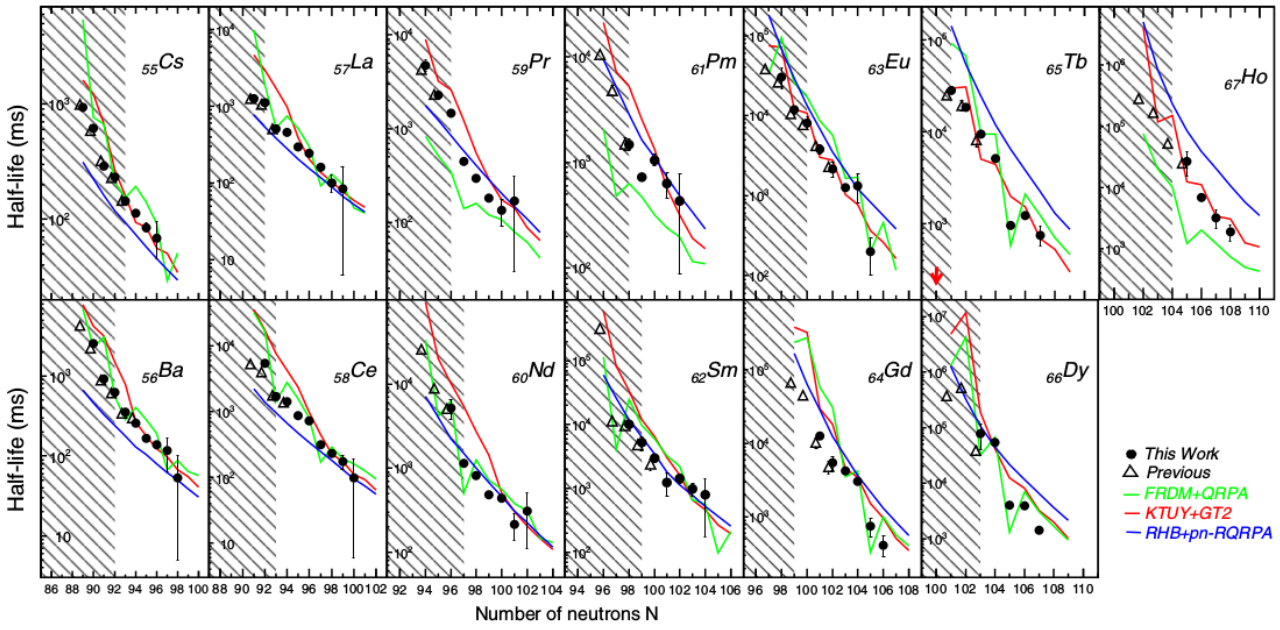

Figure 7: Systematic trends of β-decay half-lives measured by EURICA's campaign black dots [19]. Experimental values prior to EURICA white triangles [14]. The measurements are compared to predictions of three theoretical models: FRDM + QRPA [12] (green), KTUY + GT2 [22](red), and RHB pn-RQRPA [23] (blue). The shaded areas are the known-masses region at the time publication of the article.

This slight difference in the set ups, allowed BRIKEN collaboration to obtain higher statistics for the neutron rich nuclei further away from stability and even measure, for the first time, β decay half-lives of some nuclei. EURICA's measurement's had larger statistics for nuclei closer to stability. This will have an effect on the statistical errors found whilst determining the half lives of the different nuclei (See subsection 5.3).

NP1612RIBF148 experiment was divided in three different experimental campaigns that will make a total of 10 days of beam time [27]. In June 2017, an exploratory run was carried out. This exploratory run was centered on ^{167}Sm and used a total of 2.5 days of beam time. This run provided data for half-lives measurements in the region from Gd to Pm. However, the statistics for precise measurements of P_n values were rather poor, so a less exotic set up was chosen for latter campaigns. In October 2018, another experimental run was carried out using a total of 5 days of beam time. This time, the setting was centered around ^{165}Pm, and it provided measurements of half-lives and P_n values in the region form Ce to Eu. One quarter of the beam time is still available, a third experimental campaign will be focused on ^{155}La covering in this way the lowest atomic mass nuclei involved in the REP formation. This experimental campaign is expected to occur late 2019.

This master's thesis consists on a preliminary data analysis of the NP1612RIBF148 experiment that took place in October 2018. With this data analysis preliminary half-life values for nuclei from Ce to Nd were calculated. For that data analysis, a C++ software program was implemented form scratch during the making of this project. Prior to the analysis of 2018's experiment, the data from June 2017's experiment was analyzed. The analysis of 2017's experiment allowed the core implementation of the software analysis program. Only the values of the half-lives for $^{154,156-158}Ce$, $^{155-159}Pr$ and $^{158-161}$Nd, obtained from October's campaign will be reported in the present document.

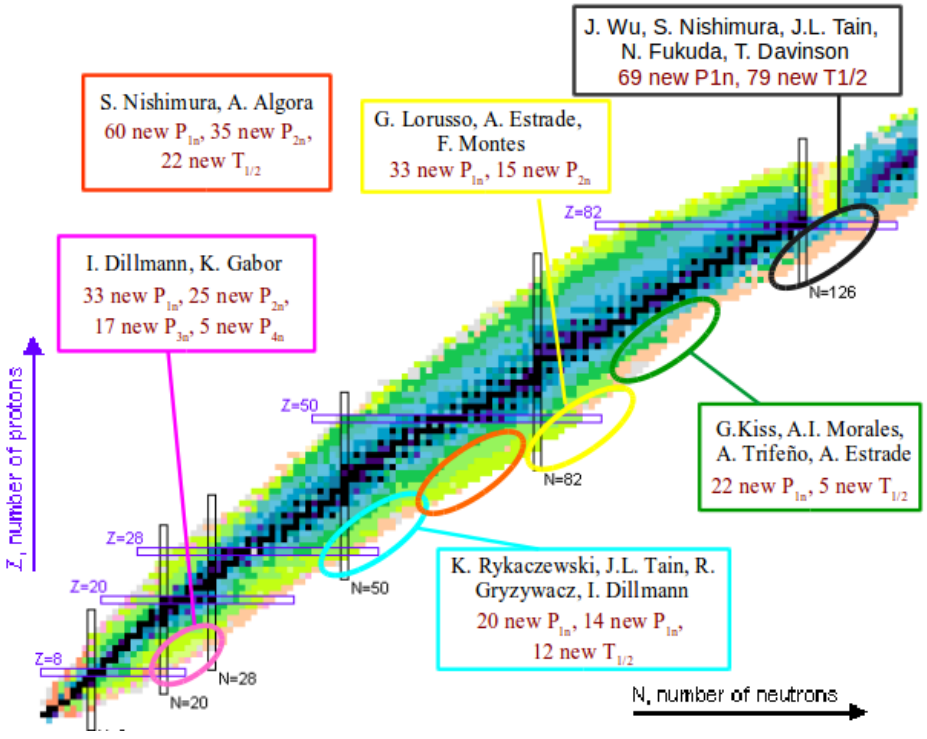

Figure 8: BRIKEN accepted proposals at RIKEN, Nishina Center.

2. Experimental Set Up

This section gives an overview of the experimental set up used by the BRIKEN collaboration when measuring nuclear properties of neutron rich nuclei in the r-process path. Special attention will be placed on the three main detection systems involved in the measurements, BigRips, AIDA and BRIKEN. Subsection 2.1 presents the basic information about the production of the Radioactive Ion Beam (RIB), as well as an overview about Big-RIPS and ZDS. Subsection 2.2 describes the active stopper detector, AIDA. In subsection 2.3 some insight will be given into BRIKEN neutron counter. Each one of this systems counts with its own DAQ system, subsection 2.4 shortly explains how the data from the different DAQs is treated and merged for the subsequent data analysis.

2.1 Primary beam production and Big-RIPS.

A ^{238}U beam is extracted from the ion source and accelerated in a multistage accelerator complex. The accelerator chain at RIBF comprehends RIKEN Heavy Ion LINAC 2 (RILAC2), RIKEN Ring Cyclotron (RRC), Fixed-frequency Ring Cyclotron (fRC), Intermediate-stage Ring Cyclotron (IRC), and Superconducting Ring Cyclotron (SRC). In Figure 9 an schematic representation of this accelerator chain can be found. At the exit of the SRC accelerator, the ^{238}U has reached an energy of 345 MeV and it has a charge state of 86^{+}. At this point, the beam impinged a ^{9}Be target, producing secondary beams by in-flight fission.

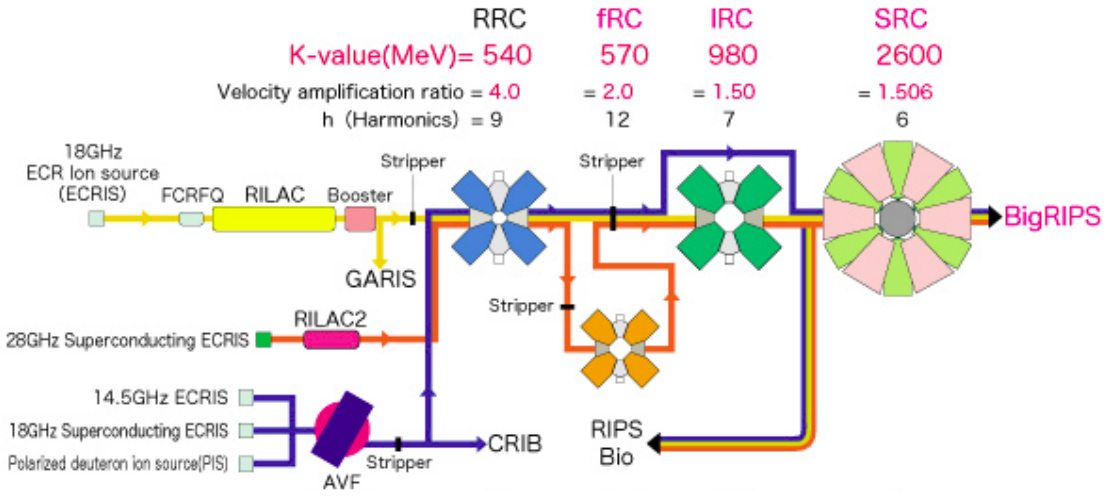

Figure 9: Schematic diagram of the accelerator chain system in this experiment. From [29]

The fission fragments of ^{238}U beam are collected by the BigRIPS separator. Figure 10 shows an schematic representation of the Big-RIPS separator + ZDS. The BigRIPS separator is designed to be a two-stage RI beam separator [30]. The first stage of BigRIPS, goes from F0 (position of the ^{9}Be target) and F2 focal planes. This stage serves for beam separation. The second stage of Big-Rips, which is defined between F3 and F7 focal planes, is employed together with the Zero Degree Spectrometer (ZDS), which goes from F7 to F11, is used to identify all the fragments transmitted through the beam line. The basic principle

of the beam separation at BigRIPS is based on the fact that charged particles with different mass-to-charge ratios (A/Q) and momenta (p) have different trajectories in magnetic fields applied by room-temperature dipoles. By placing beam-line detectors at the focal planes along BigRIPS and ZDS, one can determine the atomic number (Z) and the mass-to-charge ratio (A/Q) of the fragments. In order to do that a standard $\Delta E - B\rho - TOF$ technique was used [31].

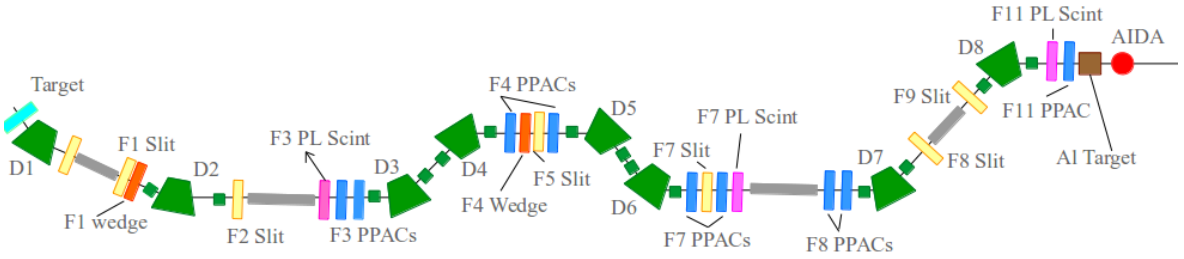

Figure 10: Schematic representation of Big-RIPS and ZDS. Note: not all the elements are present in this scheme, only the relevant ones for the current section.

2.2 Advanced Implantation Decay Array, AIDA.

After the fragment separation performed by BigRIPS, the particle beam is implanted on the Advanced Implantation Decay Array (AIDA) [36]. The implantation detector AIDA consists in a stack of six silicon double-sided strip detectors (DSSD), placed one in front of the other, with a spacing of 10 mm between them. Each DSSD has a thickness of 1 mm and an area of 71.68 mm 71.68 mm, with 128 strips 0.51 mm wide on each side (See Figure 11). This allows a stunning spatial resolution but makes the implementation of the electronics and the data analysis very challenging. The strips on each side of the DSSDs are place perpendicularly so spatial resolution in both planes, X and Y, can be obtained.

One of the challenges faced by AIDA is the accurate correlation of implantation-decay events [36]. Heavy ions are implanted in the DSSD stack and subsequently undergo radioactive decay, emitting low-energy β particles, protons, α particles, neutrons and γ rays. The neutrons and γ-rays leave the silicon undetected, and they are measured by other detection systems. The energy deposited by the heavy ions can be as high as 20 GeV, whilst the decay products have energies in the range of tens of keV to MeV. Two types of electronics are used to process the signals from each strip. For energies of the order of GeV, corresponding to implanted nuclei, the low gain branch of the electronics is used, whereas the high-gain branch is used for lower energy events such as β particles emitted in the decay of the radioactive ions. These allows implantation and decay signals to be processed differently. A plastic scintillator detector of 10mm thickness (AIDA plastic) is positioned downstream the DSSDs in the beam axis to detect particles that are not implanted in AIDA.

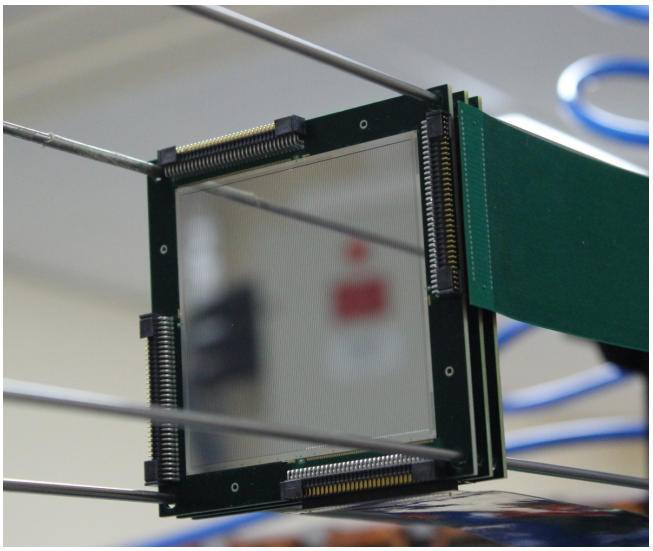

Figure 11: Picture of one of AIDA's DSSDs. AIDA is comprised of six DSSD, one in front of the other. Each DSSD has 128x128 strips (16384 pixels). Picture from [37].

2.3 BRIKEN Neutron Counter.

As aforementioned the BRIKEN collaboration aims to measure the decay properties of neutron rich nuclei such as the half lives and P_n values. The neutrons emitted from the β-delayed neutron emissions will not be able to be measured by the AIDA's DSSDs, and so another detector was needed. The BRIKEN neutron counter consists in 140 ^3He filled proportional tubes embedded in a HDPE (High Density Polyethylene) moderator matrix [38]. The total size of this matrix is 90x90x75 cm^3 with a longitudinal hole (in the beam direction) of section 11.6 cm x 11.6 cm. The lateral sides and the top are covered with 1 mm thick Cadmium sheets and additional slabs of HDPE of 25mm for neutron background attenuation. Two HPGe segmented detectors (clovers) are embedded into the HPGE moderator, transversely to the beam direction. The clover detectors are of the CARDS array type and allow for a high precision gamma spectroscopy [40]. In figure 12 a 3D model of the detector can be found.

The idea behind this neutron detector is a classical idea. The energies of the emitted neutrons can range from a few eV up to a few MeV. In order to efficiently detect them, they have to be slowed down. For that reason, the 140 ^3He tubes are embedded in the polyethylene matrix. Neutrons with lower energies will be detected by the tubes closer to the center whereas more energetic neutrons will be detected by the exterior tubes. The main disadvantage of this idea is the need of having a very long detection time (around 200 μs) due to the moderation times.

The design of this detection system was not an easy task, it had to assure the obtention of a maximum detection efficiency as well as the lowest energy dependence possible. For that, the response of the neutron detector was obtained from systematic Monte Carlo simulations implemented in GEANT4. Details about these simulations and the robustness of the algorithm can be found in [38]. In figure 13 one can see a representation of the efficiency as a function of the energy. Up to 1 MeV the total efficiency has an average of 67.9% and varies within a $\pm$1.5%. The efficiency drops to 61.1% at 2.5 MeV and to 52.0% at 5MeV.

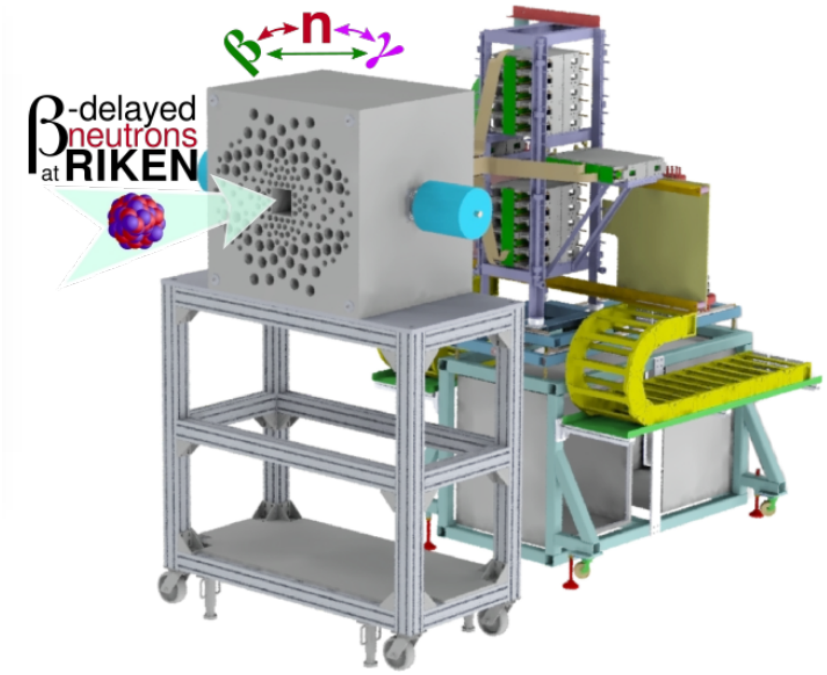

Figure 12: 3D representation of BRIKEN's experimental set up. The cubical element at the front is BRIKEN neutron counter. The different dark gray holes correspond to the ^3He tube's positions. The cylindrical light blue elements are the clover detectors. The element behind BRIKEN neutron counter is AIDA's suport system. Aida is introduced inside BRIKEN from behind. From [39].

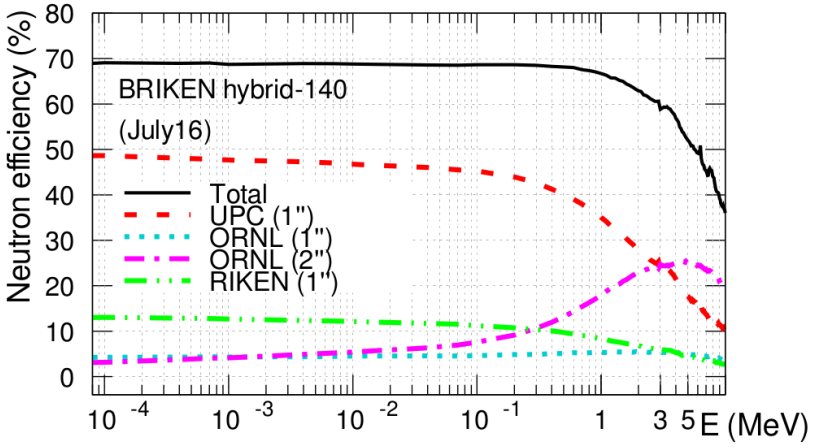

Figure 13: Neutron detection efficiency of BRIKEN's neutron counter as a function of the energy. The arrangement used at this moment consists in 140 tubes coming from some of the institutions, RIKEN [26], UPC [41], and ORNL [42].

2.4 Data Acquisition and Sorting.

As has been mentioned in this section, three main systems are necessary for the measurement, BigRIPS, AIDA and BRIKEN. Each one of this systems has its own Data Acquisition System (DAQ). In order to perform a complete analysis of the experimental data it is necessary to combine the information from the three independent DAQs. This is possible thanks to the use of a common synchronization signal distributed to all three systems. An scheme of the data structure can be found in Figure 14.

The data is taken in bunches of 1 hour called runs. A new run is started every hour and the previous run is copied to a dedicated server. To be able to follow the progress of the measurement and to detect issues that might need correction during the experiment an efficient scheme of data processing was implemented. One can then speak of three different stages in the data analysis, On-line, Near-Line and Off-Line data analysis.

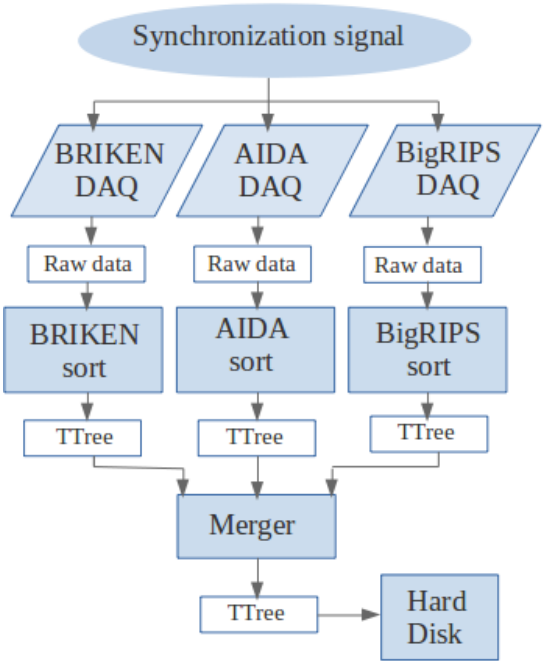

Figure 14: Diagram of the process for data merging. From [44].

Each detection system measures the events independently. Each DAQs counts with the possibility of visualizing the data as it is being taken, this is the so called On-Line analysis. If any issue is encountered by the detectors, it will be able to be detected immediately. Nevertheless, the On-Line analysis doesn't give information about the overall experimental outcome, since a combination from all the detectors is needed. After each run is finished, the raw data from this systems is processed by its dedicated sorting program and stored in the form of ROOT TTree files [43].

In order to reconstruct decay curves it is necessary to merge the time stamped data stream from each detector (raw data TTree files). This is achieved by means of the Merger software. This program was developed by the team in Valencia [44], it uses C++ to efficiently merge

the data. The output is a single TTree containing the correlation vectors of the complete data stream, necessaries for the data analysis. After every run, a fast merging of the data files is done. The conditions for this merging might not be the most efficient ones, but in this way the overall status of the experiment can be controlled. The analysis of this data is called the Near-Line analysis.

For the purpose of the present analysis, the merged data from the Near-Line analysis was processed by another software program, the AnaMerger, implemented by the team in Valencia [44]. This program classifies the correlation vectors by isotope. In this program a final selection of the products can be carried out. As an output from program, ROOT::TH1D and ROOT::TH2D histograms are obtained. These histograms contain all the necessary information for calculating the sought after nuclear properties

A proper data analysis implies a detailed study of the data at each step, and the selection of the most appropriate parameters for the sorting programs. This implies the systematic study of the effects of the different parameters and conditions needed for data processing. The analysis of the data when all the sorting steps have been carefully studied is what is considered the Off-Line data analysis. For the purpose of this project the Near-Line data was used. The sorting of the data from the different DAQs was processed during the experimental run that took place in October 2018. The merging of the files for the results present in this report was done in February 2019.

3. Data Analysis Systematic.

The main purpose of this analysis was to obtain the half-lives of $^{152-158}Ce$, $^{155-160}Pr$ and $^{157-162}Nd$. In order to obtain such values, a C++ software program was implemented from scratch. This program uses the merged data files, as indicated in 2.4, and calculates the half-lives of the nuclei of interest. This section will explain, conceptually, how this program obtains the half-lives from the corresponding correlation histograms. For that, subsection 3.1 will begin by introducing the basic mathematical formalism needed for the analysis. Subsection 3.2 will tackle the background sources and how the program deals with them. Subsections 3.3 and 3.4 will explain how the statistical errors and the β efficiencies are calculated. A detailed description of the implementation of the program itself and its usage can be found in Appendix A.

3.1 Half-Life determination: Basic Formalism

Because of the nature of the nuclei under study, the most favorable decay method was β^- decay. The daughter nucleus populated via β-decay was still radioactive, due to the large neutron excess. Likewise, the grand-daughter of the nucleus, grand-grand daughter and so on. The correlation methods used by AIDA's sorting program are able to associate each implant to its emitted β particles. But it is not possible to distinguish from which of the isotopes in the implant's decay chain the β particle has been emitted from.

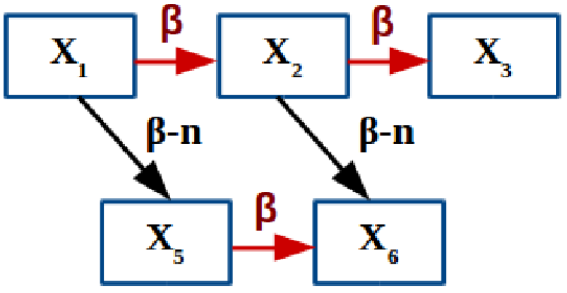

Figure 15: Schematic view of the decay chain considered in the analysis program.

For this reason, the time distribution of the beta particles relative to the associated implants was modeled taking into account not only the contributions from the parent nuclei but also the contributions of the nuclei produced in its decay chain. Figure 15 illustrates an schematic view of the decay channels involved in the half life calculation (for an abstract decay chain starting from an arbitrary nuclei $^{Z}_{A}X_1$).

Figure 7, in Section 1.5, shows the systematic trends of the half-lives measured by EURICA's campaign. The half-lives of the nuclei of interest for our analysis ($^{152-158}Ce$, $^{155-160}Pr$ and $^{157-162}Nd$) are of the order of hundreds of ms. If we follow its decay chains in figure 7, we observe how the half lives of the grand-daughter nuclei (X_3, X_6) were already long enough for it's contribution to be negligible in most cases.

The formalism describing the abundances and activities in a decay chain as a function of time are the so called Bateman equations [45]. The mathematical formulation of the equations in this case would be the following:

$$\frac{dX_1}{dt} = -\lambda_1 \cdot X_1$$
$$\frac{dX_2}{dt} = -\lambda_2 \cdot X_2 + \lambda_1 \cdot X_1 \cdot P_{\beta 1}$$
$$\frac{dX_3}{dt} = -\lambda_3 \cdot X_3 + \lambda_2 \cdot X_2 \cdot P_{\beta 2}$$
$$\frac{dX_5}{dt} = -\lambda_5 \cdot X_5 + \lambda_1 \cdot X_1 \cdot P_{\beta n 1}$$
$$\frac{dX_6}{dt} = -\lambda_6 \cdot X_6 + \lambda_5 \cdot X_5 \cdot P_{\beta 5} + \lambda_2 \cdot X_2 \cdot P_{\beta n 2}$$

In these equations X_1 is an abstract arbitrary nuclei with atomic and mass numbers Z and A respectively. If $X_1 = {}^{A}_{Z}X_1$ then $X_2 = {}^{A}_{Z+1}X_2$, $X_3 = {}^{A}_{Z+2}X_3$,$X_5 = {}^{A-1}_{Z+1}X_5$ and $X_6 = {}^{A-1}_{Z+2}X_6$. λ_i is the corresponding decay constant of the X_i nucleus. The decay constant is related to the half life as follows:

$$\lambda = \frac{ln2}{T_{1/2}}$$

$P_{\beta i}$ and $P_{\beta n i}$ refer to the β and β-delayed neutron emission probabilities respectively. The initial conditions for solving this equations are the following:

$$X_1(t=0) \;=\; X_0$$
$$X_i(t=0) \;=\; 0, \quad i = 2,3,5,6$$

With X_0 being the initial activity of the parent nuclei. The solution of this system of equations will then be:

$$X_1 = X_0 \cdot e^{-\lambda_1 t}$$
$$X_2 = X_0 P_{\beta 1} \lambda_1 \cdot \left(\frac{-\lambda_1 t}{\lambda_2 - \lambda_1} + \frac{e^{-\lambda_2 t}}{\lambda_1 - \lambda_2} \right)$$
$$X_3 = X_0 P_{\beta 1} P_{\beta 2} \lambda_1 \lambda_2 \cdot \left(\frac{e^{-\lambda_1 t}}{(\lambda_2 - \lambda_1)\cdot(\lambda_3 - \lambda_1)} + \frac{e^{-\lambda_2 t}}{(\lambda_1 - \lambda_2)(\lambda_3 - \lambda_2)} + \frac{e^{-\lambda_3 t}}{(\lambda_1 - \lambda_3)(\lambda_2 - \lambda_3)} \right)$$
$$X_5 = X_0 P_{\beta n 1} \lambda_1 \cdot \left(\frac{e^{-\lambda_1 t}}{\lambda_5 - \lambda_1} + \frac{e^{-\lambda_5 t}}{\lambda_1 - \lambda_5} \right)$$
$$X_6 = X_0 P_{\beta 1} P_{\beta n 2} \lambda_1 \lambda_2 \cdot \left(\frac{e^{-\lambda_1 t}}{(\lambda_2 - \lambda_1)(\lambda_6 - \lambda_1)} + \frac{e^{-\lambda_2 t}}{(\lambda_1 - \lambda_2)(\lambda_6 - \lambda_2)} + \frac{e^{-\lambda_6 t}}{(\lambda_1 - \lambda_6)(\lambda_2 - \lambda_6)} \right)$$
$$+ X_0 P_{\beta n 1} P_{\beta 5} \lambda_1 \lambda_5 \cdot \left(\frac{e^{-\lambda_1 t}}{(\lambda_5 - \lambda_1)(\lambda_6 - \lambda_1)} + \frac{e^{-\lambda_5 t}}{(\lambda_1 - \lambda_5)(\lambda_6 - \lambda_5)} + \frac{e^{-\lambda_6 t}}{(\lambda_1 - \lambda_6)(\lambda_5 - \lambda_6)} \right)$$

The total number of decays per unit time as a function of time is obtained by summing the different contributions, which gives:

$$\frac{N_\beta}{dt} = -\sum_i \lambda_i X_i(t) + C(t) \tag{3}$$

The index i = 1,2,3,5,6 refers to the nuclei taken into account in the decay chain. C(t) represents the background. The previous equations depend on several parameters, such as the different decaying constants (λ_i), the β emission probabilities ($P_{\beta i}$), the neutron emission branching ratios ($P_{\beta ni}$) and the initial activity of ${}^{A}_{Z}X_1$. The initial activity and the half life of the parent nuclei (X_0 and $T_{1/2} = ln2/\lambda_1$) were obtained by fitting Eq.3 to the experimental decay spectrum. All the other parameters were adopted, if available, from either predicted or experimental data (EURICA's measurements).

3.2 Background Corrections.

Several background sources can affect the correlation histograms and can limit the minimum detectable activity. We will call uncorrelated β-background to counts appearing in the histograms that come form accidental implant-β correlations. This uncorrelated background has been found to have a time-dependent distribution due to beam instabilities and pauses [44]. For the present analysis this time distribution won't be noticeable due to low statistics. Statistical fluctuations will hinder any time dependence of the background. Figure 16 shows the implant β correlation histogram. From this image we can clearly observe how the uncorrelated background can be easily fitted to a constant polynomial. For the half-life calculations, the background is introduced into the fit function as another input parameter (In Eq. 3 is parameter C(t)).

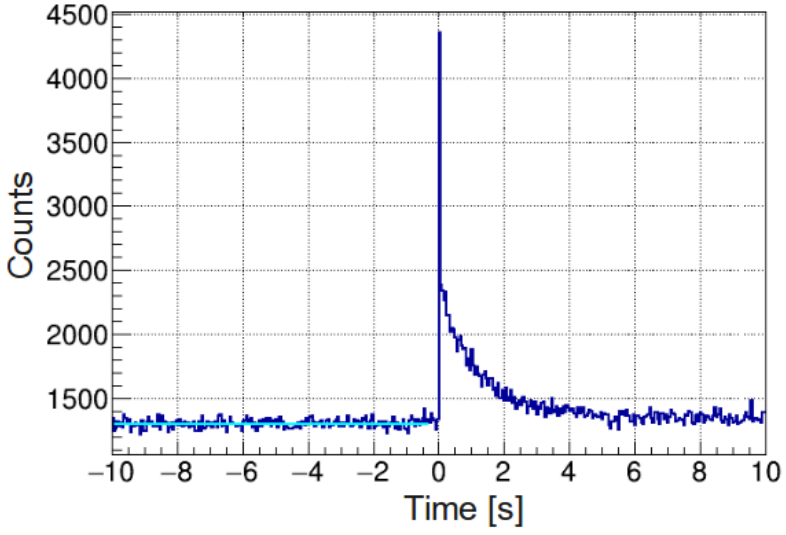

Figure 16: Implant-β decay curve for ^{160}Nd. Light Blue, fitted constant background.

In figure 16 we can clearly observe a prominent spike at t=0, this spike was present in every correlation histogram involving AIDA's data. This spike does not represent the reality, it is an artificial construction coming from AIDA's sorting program. It must be noted that the sorting of AIDA's data for the present analysis was done using Lucky-Doll sorting program [46]. The way the software program implemented for this work dealt with this problem, was by ignoring the t = 0 bin in every histogram. The unreal number of counts for this bin will still be present when representing the decay curves, but it's effect in the calculated half-lives will be negligible. In the following chapter, in particular, in subsection 4.4, the effects this spike has in half-life calculation is shown.

3.3 Statistical error determination.

The uncertainty when calculating the half lives and initial activities for the different nuclei came mainly from the uncertainties of the parameters that contribute to the fit. As indicated in section 3.1, the parameters needed for the fitting procedure are the half-lives (or decay constants) of all the nuclei involved in the decay chain. Also, the branching rations, or neutron emission probabilities are necessary. The half-life and the initial activity of the parent nuclei will be set as free parameters and obtained with ROOT's TH1::Fit [43] method. In particular, for the present analysis the binned maximum likelihood was used.

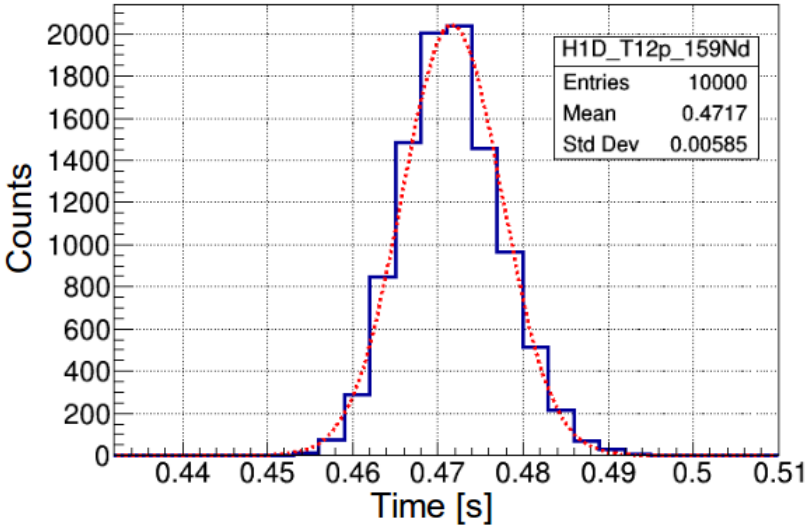

Figure 17: Output histogram of ^{159}Nd's half-life after a thousand repetitions.

The values of the half-lives needed for the present analysis were all taken from ENSDF (Evaluated Nuclear Structure Data File Search and Retrieval) [14]. Most of these values were experimentally measured by EURICA's campaign at RIKEN [19] in 2017. These parameters were introduced into the program as random Gaussian variables (ROOT::TRandom3::Gaus) with mean values and errors as indicated in ENSDF. The neutron emission probabilities for these nuclei had never been experimentally measured, so theoretical values had to be used. The values used were the ones given by P. Möller in 2003 [12].

The analysis program is executed 1000 times, from each execution a value of the parent's half-life and initial activity is obtained. These values are introduced in 1D histograms, which are fitted to a Gaussian distributions once the thousand executions are finished. Figures 17 and 18 show the output of the half-life and X_0 calculation for ^{159}Nd. Two other minor sources of errors were also taken into account. Those are the errors coming from the fitting method itself, particularly the fitting of the final Gaussian distribution. The uncertainty is calculated as indicated in Eq. 4. Where $\Delta_{T1/2}$ is the sigma of the parameter's Gaussian, Δ_{mean} is the error when calculating the mean and Δ_{error} is the error when calculating the sigma. The main contribution to the error comes from Δ_{T12}.

$$Err = \sqrt{\Delta_{T12}^2 + \Delta_{mean}^2 + \Delta_{error}^2} \tag{4}$$

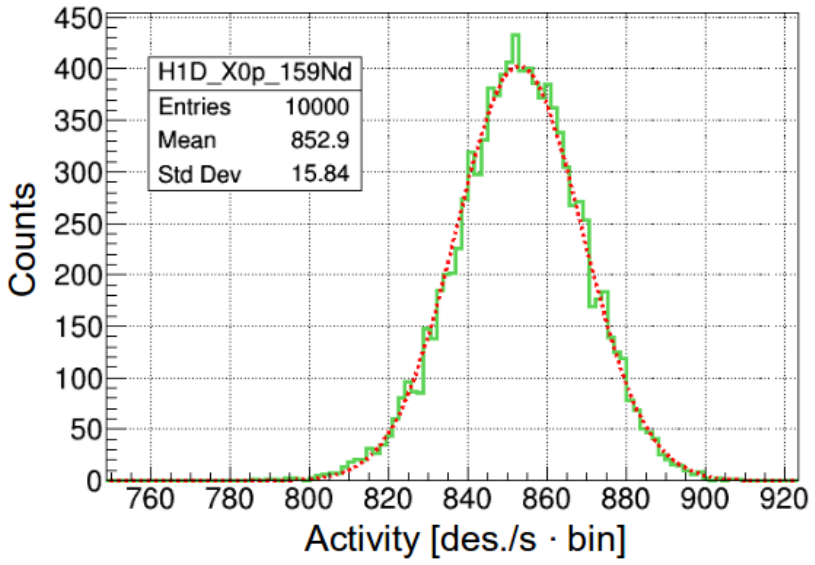

Figure 18: Output histogram of ^{159}Nd's initial activity (X_0) after a thousand repetitions.

3.4 β-Efficiency: Concept and Calculation.

All nuclei implanted into AIDA will undergo radioactive decay, but not all the electrons emitted will be properly measured. The detection efficiency will depend on the electron's energy, the implantation depth and position, and the reconstruction method for β events. Since the Q_β value (maximum possible energy of the electron) varies from one nuclei to the other, the detection efficiency will also be different for each nuclei. It is not easy to determine experimentally the detection efficiency for every decay. In the present analysis the β-efficiency was calculated as follows: For each nuclei, the total number of implants can be calculated by integrating the number of counts from the PID plot at AIDA's focal plane, we call this N_{imp}. Now, from the fitting procedure we have obtained the value for the initial activity of each parent nuclei. This initial activity can be used to calculate the β-efficiency in the following way:

$$\beta_{eff} = \frac{X_0}{N_{imp} \cdot Bin_{width}} \tag{5}$$

In this case , X_0 must be divided by the bin's width in order to obtain the β-efficiency because of how the program was implemented. One of the parameters that need to be adjusted in AIDA's sorting program is the so called energy threshold. This threshold refers to the minimum energy below which detected β-particles will not be considered. This threshold can be adjusted depending on the interests of the data analysis. Variations in this value can make β-efficiencies vary from $30 - 42\%$ (low threshold) down to $20 - 26\%$ (high-threshold). Deciding which is the most convenient threshold in AIDA's sort is challenging, people are actively working in improving the sort conditions for the different experiments [20] [21].

4. Fake data program testing.

In order to cross check the reliability of the results obtained by the implemented data analysis program, the software was thoroughly tested on artificially generated data. The advantage of fake data program testing is the availability to cross check the values obtained from the analysis with the exact solution. In this section, the most remarkable results form the fake analysis testing have been summarized. In subsection 4.1 a simple example of half life calculation from a histogram with no statistical fluctuations and a good noise to signal ratio can be found. Subsection 4.2 shows the effects reducing the ratio between initial number of implants and background has on the half-life calculations. The effect statistical fluctuations have on the reliability of the results is shown in subsection 4.3. Subsection 4.4 ends up exploring the effects the 20ms bump (explained in section 3.2) has on the results.

4.1 Half-Life Determination.

As a first example, let's imagine a nuclei with N = 96 and Z = 60. The values used for the half-lives and P_n values needed to generate the corresponding implant-β decay histogram have been summarized in table 1. The notation followed is the one introduced in section 3.1. With this parameters a decay curve was generated, and introduced as the experimental implant-β histogram into the implemented code.

X_0	$T_{1/2}(1)$	$T_{1/2}(2)$	$T_{1/2}(3)$	$T_{1/2}(5)$	$T_{1/2}(6)$	$P_n(1)$	$P_n(2)$	$P_n(5)$	Back
180	1.5	8.2	10.8	10.1	12.1	0.5	0.1	0.3	10

Table 1: Parameters used for the generation of the fake implant-β correlation histogram. Half lives are expressed in seconds. To clarify the notation: $T_{1/2}$(i) and P_n(i) stand for the half-life and P_n value of X_i respectively. Back, stands for background.

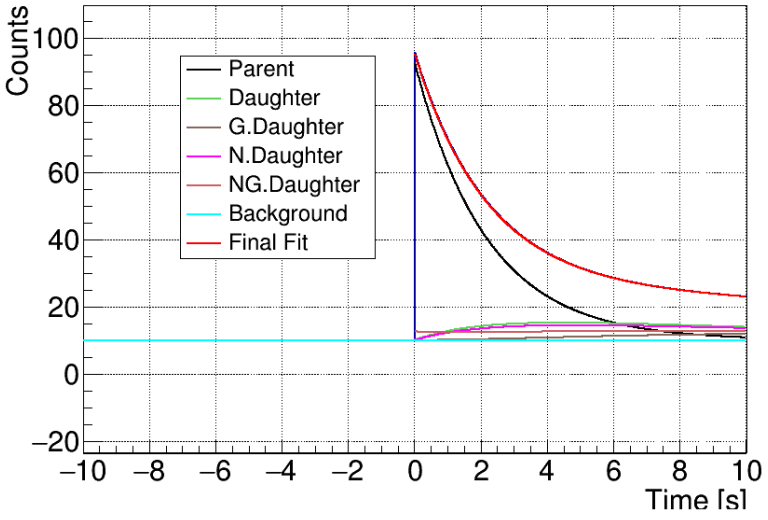

Figure 19: Fitting curve of the artificially-generated implant-β beta decay curve. Parameters used for this simulation are the ones in Table 1.

The expected $T_{1/2}$ and X_0 were 1.4 s and 180 counts respectively. The values obtained from the simulation were 1.415(22) s for the half life and 179.7(35) for the initial activity. Both parameters show a good agreement with the expected parameters. In figure 19 one can see how well the fitting curve agrees with the artificially generated histogram.

4.2 Effects of X0 in Half-Life determination.

The fitting program is trying to determine simultaneously X_0 and $T_{1/2}$. It is not unreasonable to think that an extreme value for the initial activity might affect the calculation of the half-life. The initial activity is directly related with the number of implants of that nuclei reaching AIDA, and thus, to the statistics available for such nuclei. What is important is the relative ratio between the number of implants and the uncorrelated background. To study this effect the background was maintained constant at 10 counts while the value of the initial activity was modified. Three illustrative examples of the generated histograms have been represented in figure 20.

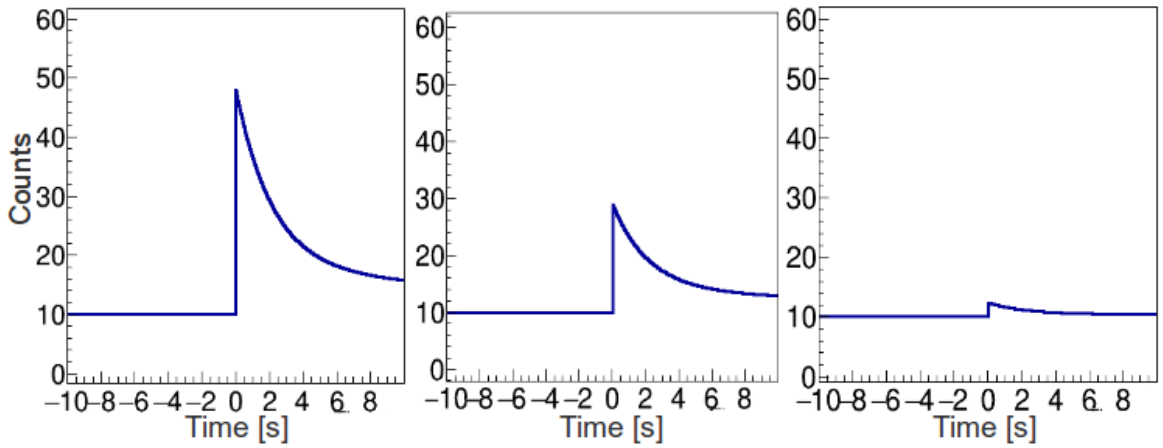

Figure 20: Comparison of three artificially generated histograms, for three different values of X_0. From left to right $X_0 = 80$,$X_0 = 40$, $X_0 = 5$ The other parameters are the ones indicated in table 1.

The results show that the implemented program presents no problem when calculating the half-life even in the worst scenario. Even so, reducing the ratio between the initial number of implants (X_0) and the uncorrelated background increases considerably the relative error of the fitted parameters. Figure 21 shows clearly this effect.

4.3 Effects of statistical fluctuations in Half-Life determination.

An effect that has not been considered in the previous cases is the statistical fluctuation. In order to recreate this fluctuations, for each bin of the implant-β decay histogram a Gaussian random variable was generated, the value generated following the model indicated in Section 3.1, and a σ that could be easily modified. This statistical fluctuations are closely related to the initial number of implants of that nuclei, and thus to X_0. For that reason, the value of σ was chosen to be the one indicated in equation 6.

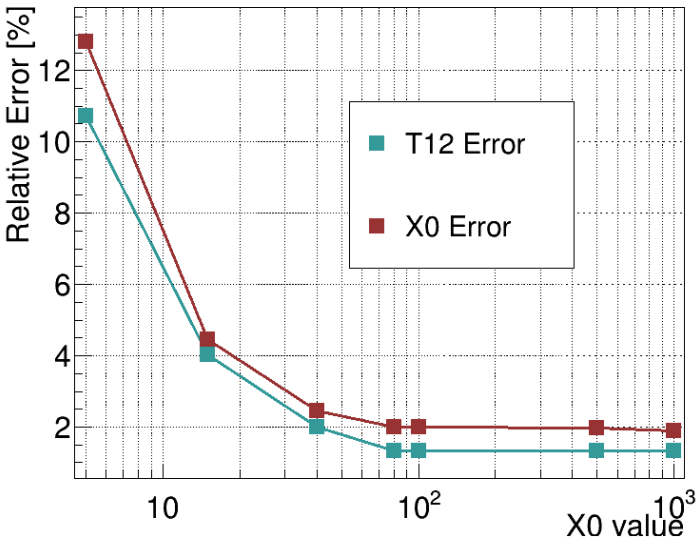

Figure 21: Representation of the relative errors when calculating $T_{1/2}$ and X_0 for different values of X_0.

$$\sigma = 9 \cdot \frac{background}{X_0} \tag{6}$$

Equation 6 was selected as it managed to approximately reproduce the experimental statistical fluctuations. Figure 22 shows the generated histograms for three different values of X_0. From this figure we can clearly observe that for a small X_0, the statistical fluctuations can make it impossible to distinguish a decay curve.

$T_{1/2}(1)$	$T_{1/2}(2)$	$T_{1/2}(3)$	$T_{1/2}(5)$	$T_{1/2}(6)$	$P_n(1)$	$P_n(2)$	$P_n(5)$
1.42	3.75	11.4 min	18.9	12.4 min	0.0	0.0	0.0

Table 2: Parameters used for the generation of the fake implant-β correlation histogram of figure 22. To clarify the notation, T12(i) is the half life of X_i. This half lives are expressed in seconds if not indicated otherwise.

A systematic study of the effects different background/X_0 ratios had in the half-life determination was performed. For that, histograms with different background/X_0 were built and subsequently analyzed with the half-life analysis program. The values chosen for this study tried to represent the ones found in the experimental data cases. Figure 23 is representing the differences between the expected half life (1.42 s) and the one obtained with the implemented software when analyzing histograms . From this figure one can clearly infer that as X_0 decreases, the obtained half-life starts differing more and more from the expected value.

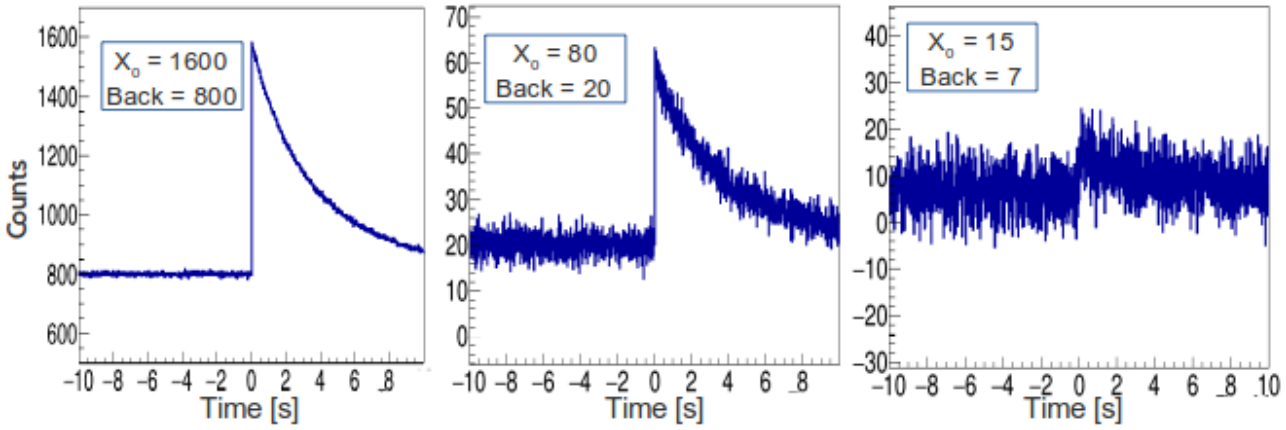

Figure 22: Comparison of three histograms with three different background/X_0 rations. The values of the other parameters are the ones in table 2.

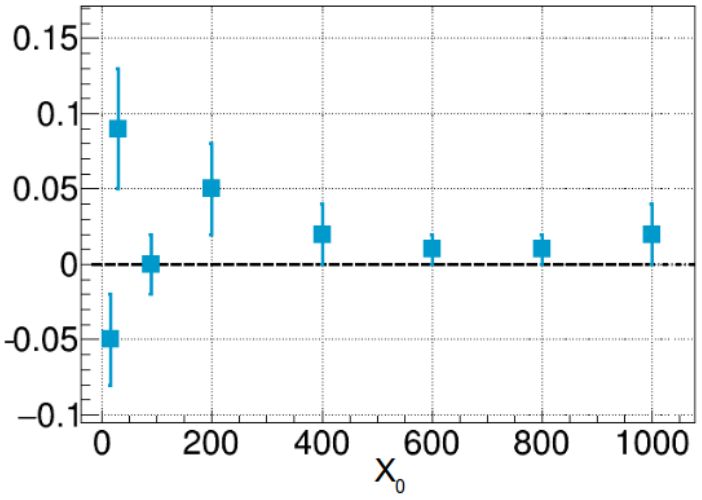

Figure 23: Differences between the expected half-life (1.42 s) and the half-lives obtained with the implemented software. For different values of X_0 when considering statistical fluctuations.

4.4 20ms bump in Half-Life determination.

A common feature, of all the correlation histograms involving AIDA's data, was a 20ms bump. This disproportionate increase in the number of counts is not a real effect as indicated in section 3.2. The analysis program implemented deals with this bump by ignoring the bin which contains time 0s. In this section we wanted to study how sensitive half-life calculations were to this 20 ms bump, and also to see up to which point ignoring the first bin was a good strategy.

In order to study this effect, a 20 ms bump was introduced in the artificially generated histograms. The number of counts of this bump was taken to be eight times the value of $X_0 \cdot \lambda_1$ to roughly simulate the experimentally obtained values. Ignoring the first bin in the decay curve might not be a big problem for those nuclei with considerably long half lives, as there is plenty of information in the subsequent bins. Nevertheless this can be a considerable

source of systematic error for nuclei with short half-lives. Figure 24 shows an example of three histograms with different half lives and with a 20 ms bump. In this case statistical fluctuations have not been taken into account.

To see the effect this bump has on half-life calculations, several histograms, with different half life values, were analyzed. Even if the fitting program keeps giving reasonable results for very short half lives, the values of the initial activity become systematically larger than the expected value. This results in poorly fitted histograms. As the half-life decreases, the fitting program becomes very sensitive to changes in the initial initial guess in X_0. Lousy selection of half-life guess also results in a poor fit results. Figure 25, clearly shows the effects, the 20ms bump has on the results, by representing the differences between the obtained values of the half lives and X_0 and their expected values.

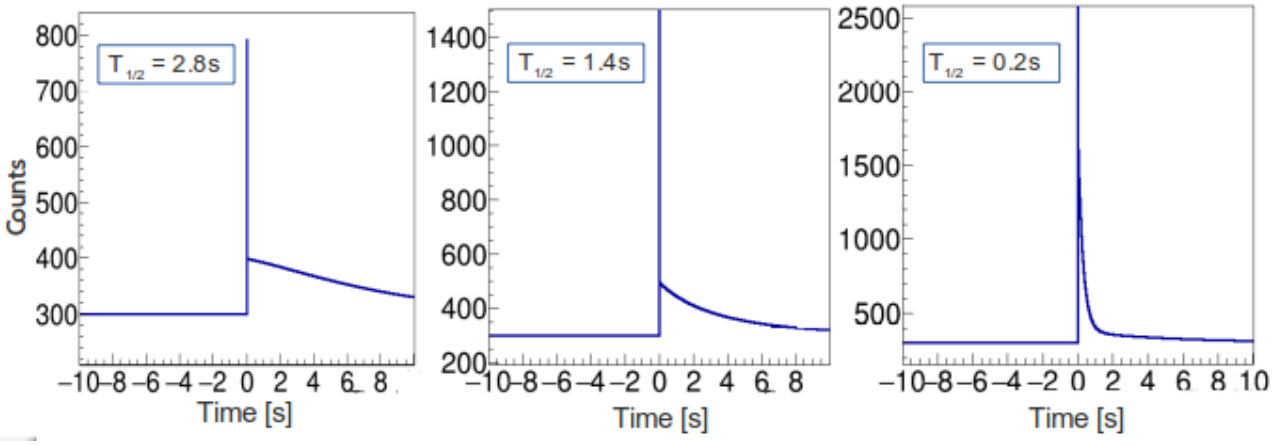

Figure 24: Artificially generated histogram with 20ms bump. Half lives and P_n values from table 2. $X_0 = 400$ in all cases.

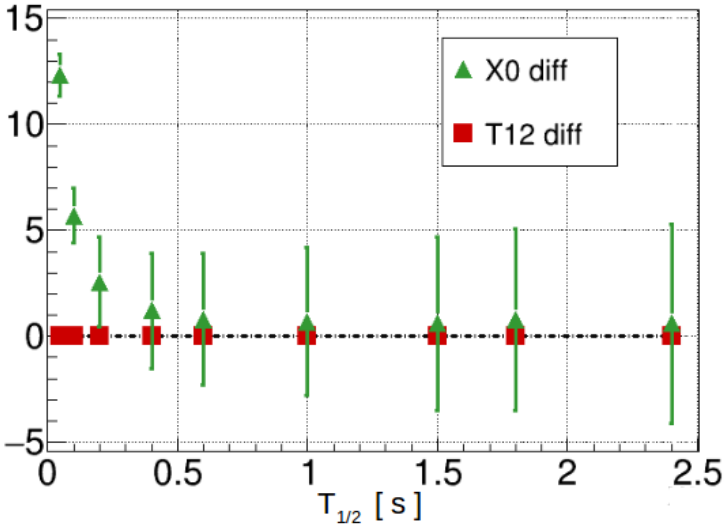

Figure 25: Differences between the expected half-lives and the ones obtained by the implemented software (red). Differences between the expected X0 and the ones obtained (green).

In none of this subsections, the effects of statistical fluctuations and half-life diminishment have been considered simultaneously. As a rule of thumb, the further away from stability the lower the production rates. This implies a smaller $X_0/Background$ ratio as well as a bigger statistical fluctuation. Furthermore, the more exotic the nuclei the shorter the half-life tends to be. The combination of this factors can make the half-life determination process very difficult and in some cases even impossible.

5. Experimental Results.

In this section, we will present the results of the analysis for the half-lives of the isotopes $^{152-158}Ce$, $^{155-160}Pr$ and $^{157-162}Nd$. The results obtained were compared, whenever available, with previously measured values (EURICA's campaign [19]) or theoretical models (Möller 2003 [12]). Subsection 5.1 gives an overview of NP1612-RIBF148 experiment, October 2018's campaign, and some experimental characteristics particular from this experiment. Subsection 5.2 includes a detailed description of half-life calculation for ^{157}Pr nuclei, as an illustrative example. This procedure was followed for all the other nuclei analyzed in this report. A summary of the results for all the nuclei analyzed can be found in Subsection 5.2.

5.1 NP1612-RIBF148 Experiment, October 2018.

The main objective of October's 2018 campaign was to provide enough data for obtaining half-lives and P_n values in the region from Ce to Eu. For that, a high intensity ^{238}U beam was accelerated up to 345 MeV before impinging on a 4-mm-thick (0.56 g/cm) ^{9}Be target. The secondary in-flight fission beam was then collected by BigRIPS (Subsection 2.1). BigRIPS setting was centered around ^{165}Pm to optimize the production rates of the nuclei of interest. In order to optimize BigRIPS setting, and to ensure produced nuclei were correctly implanted in AIDA (Subsection 2.2), detailed Lise++ [49] simulations were performed by N.Fukuda and the BigRIPS team [50]. Figure 26 shows the expected production rates (calculated with LISE++) of the nuclei analyzed in this report.

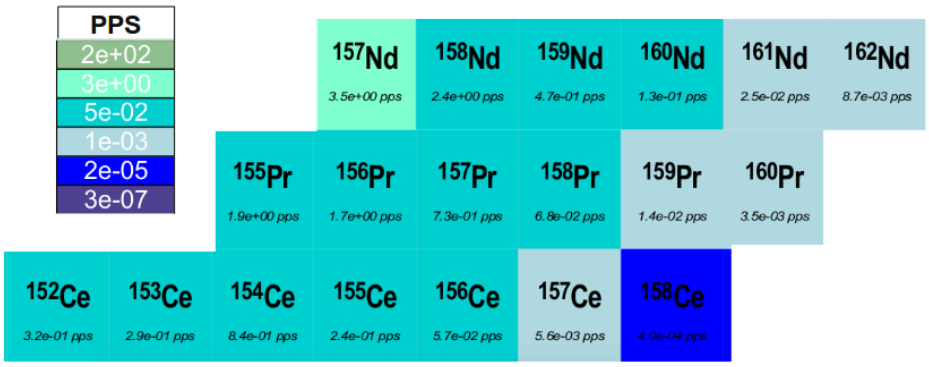

Figure 26: Lise++ production rates in particles per second (pps).

Already in Lise++ simulations, it was obvious that a full separation of the nuclei was not accomplished. The biggest problem affecting the particle identification was the presence of charge states. Figure 27 the experimental particle identification (PID) plot can be found. A first PID cleaning was applied to the particle identification plot for background reduction during the experiment. Nevertheless, for a proper data analysis a more exhaustive PID cleaning must be applied. More information abut the cleaning procedure can be found in [51].

ROOT::TCUTs were created so each isotope could be analyzed separatelly. This cuts have been represented by circles in figure 27. The experimental total number of implants was calculated by integrating the number of counts in each one of this ROOT::TCUTs. Figure 28

shows the total number of implants for each one of the nuclei analyzed in this report. October 2018's experiment was a total of 65h of beam time from which 60h have been analyzed. The observed experimental rates are considerably smaller than the Lise++ expected rates (experimental rates $\sim 5\%$ Lise++ rates). The experimental number of implants varies from $5 \cdot 10^5$ implants (for ^{158}Nd) to $8 \cdot 10^2$ implants (for ^{158}Ce). The transmission rate from F11 point to AIDA was around 70% for the nuclei of interest.

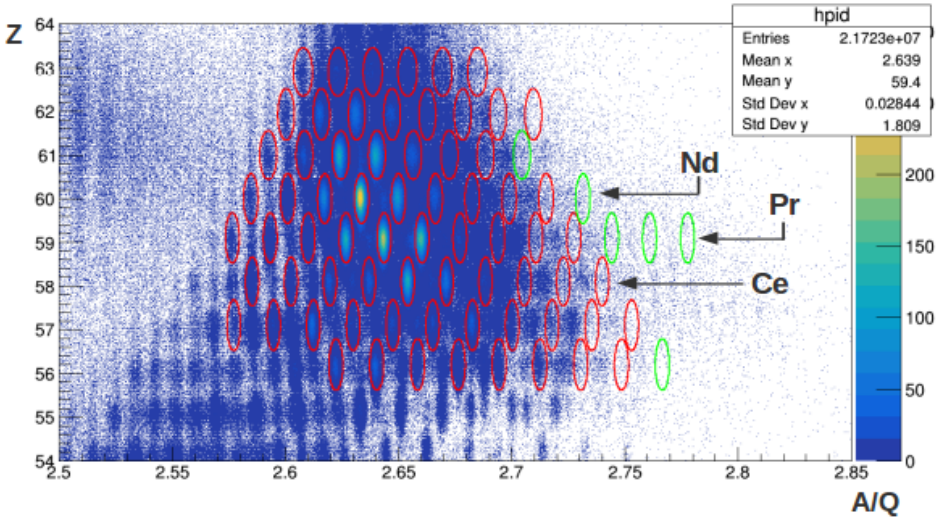

Figure 27: Particle identification plot shown as Z vs mass-to-carge ratio (A/Q) with full statistics of the experiment. At F11 focal plane. Red circles, nuclei with already known half-lives. Green circles, nuclei with unknown half-lives.

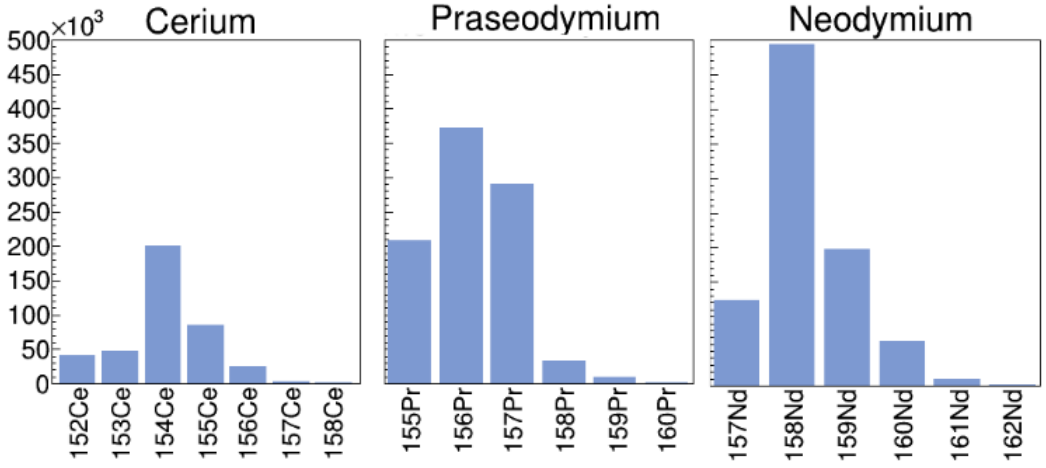

Figure 28: Number of implanted nuclei of each isotope in the DSSDs of AIDA.

In order to assure the implantation of the ions of interest in AIDA, an aluminum degrader is commonly placed at F11 focal point. For this experiment three different aluminum degraders of 2.3 mm, 2.8 mm and 3 mm were used. The stopping range is correlated to the total kinetic energy of the fragment and its stopping power in a defined material. Figure 29 shows three different implantation depth histograms. We can clearly observe that most of the implants were stopped between the third and the forth DSSDs.

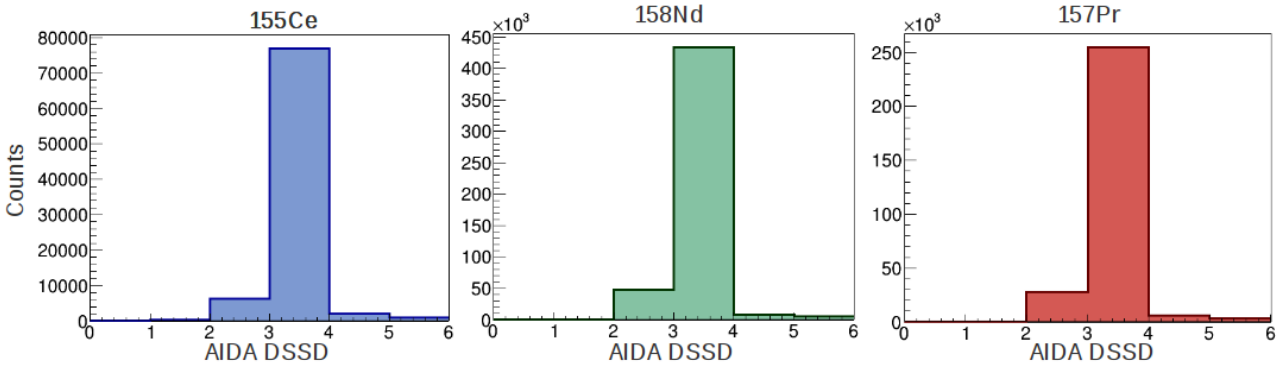

Figure 29: Implantation depth histogram of three different ions in AIDA.

The sorting program used to process AIDA's data was Lucky Doll [46]. Implant-β correlation time was selected to be 10 s. The β-efficiencies of all the nuclei analyzed for this report are summarized in Figure 30. As can be seen in this Figure, the average value of this efficiencies is around 22%. For this work the AIDA's data was processed with a high threshold setting. Once the data from the different detectors was merged, it was processed by the so called "AnaMerger_Reloaded" code. F11 and AIDA's plastic were used as vetoing signals for background reduction.

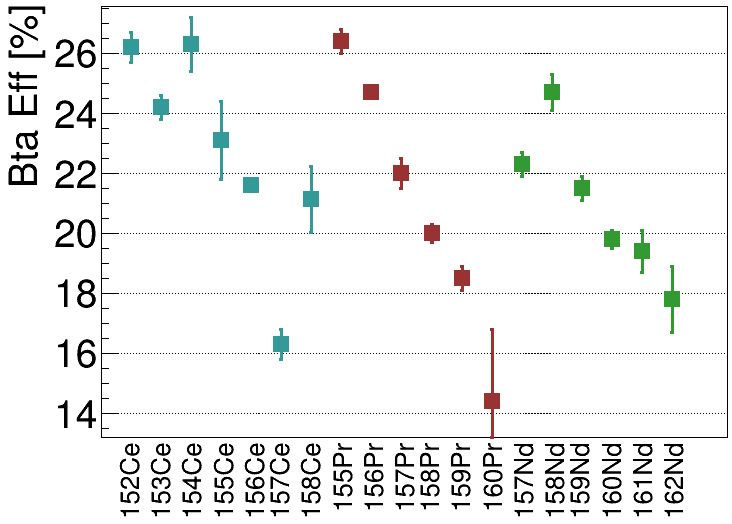

Figure 30: β efficiency in % for the nuclei analyzed for this report. The colors illustrate the different nuclei, blue for Ce, red for Pr and green for Nd.

5.2 Half-Life determination ^{157}Pr.

The number of ^{157}Pr implants measured in AIDA was around $3 \cdot 10^5$. In figure 29, one can observe how the implantation of this nuclei was mainly in the third and forth DSSDs. Transmission rate from F11 focal point and AIDA was 67%. The decay chain taken into account for this calculation is the one in figure 31. In table 3 the different values used for the

simulation had been summarized. For this nuclei, the values of the half-lives of the elements in it's decay chain had been previously measured by EURICA's campaign [19]. The values of the neutron emission probabilities were taken to be the ones calculated by Möller in 2003 [12]. Figure 32 shows the implant-β decay curve for ^{157}Pr nuclei, in dark blue, as well as the fitted curve and the different contributions of the nuclei in its decay chain.

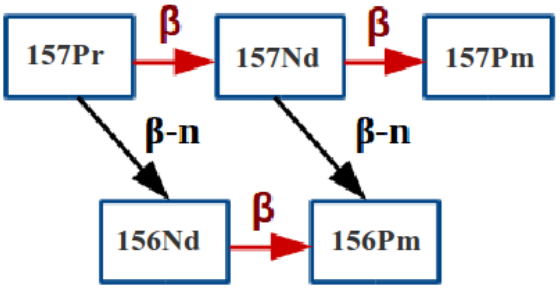

Figure 31: Decay scheme taken into account for the calculation of $T_{1/2}$ for ^{157}Pr nucleus.

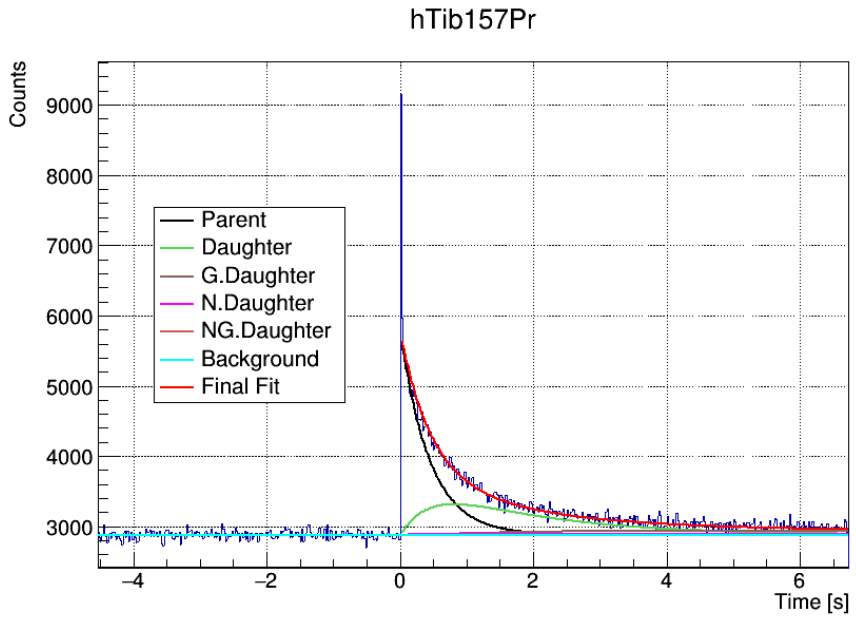

Figure 32: β-decay curve for ^{157}Pr nuclei. Total decay function is plot in red line while decoupled components are drawn in different colors. To clarify the terminology used: X_1=Parent, X_2=Daughter. X_3=G.Daughter. X_5=N.Daughter. X_6=NG.Daughter.

The value of the half-life of ^{157}Pr had been previously measured by EURICA's campaign [19]. The value obtained in that case was 0.307 (21) s. The theoretical for the half-life obtained by Möller in 2003 was 0.16047 s [12]. The present analysis yielded a $T_{1/2} = 0.318(5)$ [s] and a β efficiency measurement of around 22.3(13) %. The background value for this nucleus was 2879(1) counts. From this we can see how the value obtained with our analysis matches quite well the previously calculated experimental value. The half life obtained with Möller's theoretical calculation seems to be shorter than the experimentally measured value. In the next subsection we will see that this is a common feature for all Praseodymium nuclei.

Parameter	Value	Uncertainty	Comment
157Nd ($T_{1/2}$)	1.15	0.13	literature [19]
157Pm ($T_{1/2}$)	10.56	0.1	literature [19]
156Nd ($T_{1/2}$)	5.06	0.13	literature [19]
156Pm ($T_{1/2}$)	27.05	0.5	literature [19]
157Pr (P_n)	0.0875	0.2	literature [12]
157Nd (P_n)	0	0.2	literature [12]
157Pr ($T_{1/2}$)	0.325	0.020	BRIKEN 2018

Table 3: Summary of fitting parameters for ^{157}Pr. The column "comment" provides additional information for the parameters. For ^{155}Nd only positive values of the P_n value were considered in the simulation (from 0-0.2).

5.3 Overview of the Results.

As a summary, Tables 4, 5 and 6 exhibit the values of all the half-lives calculated for this report. Figure 33 graphically represents the values found in this tables. This results have been compared with EURICA's experimental campaign and with Möllers's theoretical values. Most of the results exhibit a good agreement with the experimental data points. Bigger discrepancies have been found when comparing this results to Möller's theoretical model. This theoretical model has been selected because of it's extensive usage. Nevertheless as shown in subsection 1.4, huge disagreements can be found between different theoretical models. Comparisons between experimentally measured half-lives and the theoretically calculated ones have to be done considering the limitations of the theoretical models.

	This Work		EURICA's Campaing		Möller
Nuclide	$T_{1/2}$	Uncertainty	$T_{1/2}$	Uncertainty	$T_{1/2}$
152Ce	1.46	0.06	1.42	0.02	2.76212
153Ce	0.897	0.017	0.865	0.0025	0.865
154Ce	0.726	0.016	0.722	0.0014	0.79931
155Ce	0.372	0.015	0.313	0.007	0.1688
156Ce	0.259	0.010	0.233	0.009	0.29
157Ce	0.194	0.010	0.175	0.041	0.19453
158Ce	0.003	0.077	0.008	0.093	0.15897

Table 4: Summary of half-lives of Cerium isotopes.

	This Work		EURICA's Campaing		Möller
Nuclide	$T_{1/2}$	Uncertainty	$T_{1/2}$	Uncertainty	$T_{1/2}$
155Pr	1.652	0.057	1.47	0.3	0.34784
156Pr	0.562	0.013	0.444	0.006	0.14166
157Pr	0.324	0.019	0.307	0.021	0.16047
158Pr	0.210	0.005	0.181	0.014	0.12113
159Pr	0.207	0.010	0.134	0.043	0.10732
160Pr	0.208	0.041	0.069	0.14	0.07983

Table 5: Summary of half-lives of Praseodymium isotopes.

	This Work		EURICA's Campaing		Moller
Nuclide	$T_{1/2}$	Uncertainty	$T_{1/2}$	Uncertainty	$T_{1/2}$
157Nd	1.142	0.032	1.15	0.13	0.50421
158Nd	0.887	0.032	0.810	0.03	1.25772
159Nd	0.504	0.024	0.485	0.039	0.71423
160Nd	0.376	0.008	0.439	0.037	0.5625
161Nd	0.260	0.009	0.215	0.076	0.38088
162Nd	0.327	0.020	0.310	0.2	0.30818

Table 6: Summary of half-lives of Neodymium isotopes.

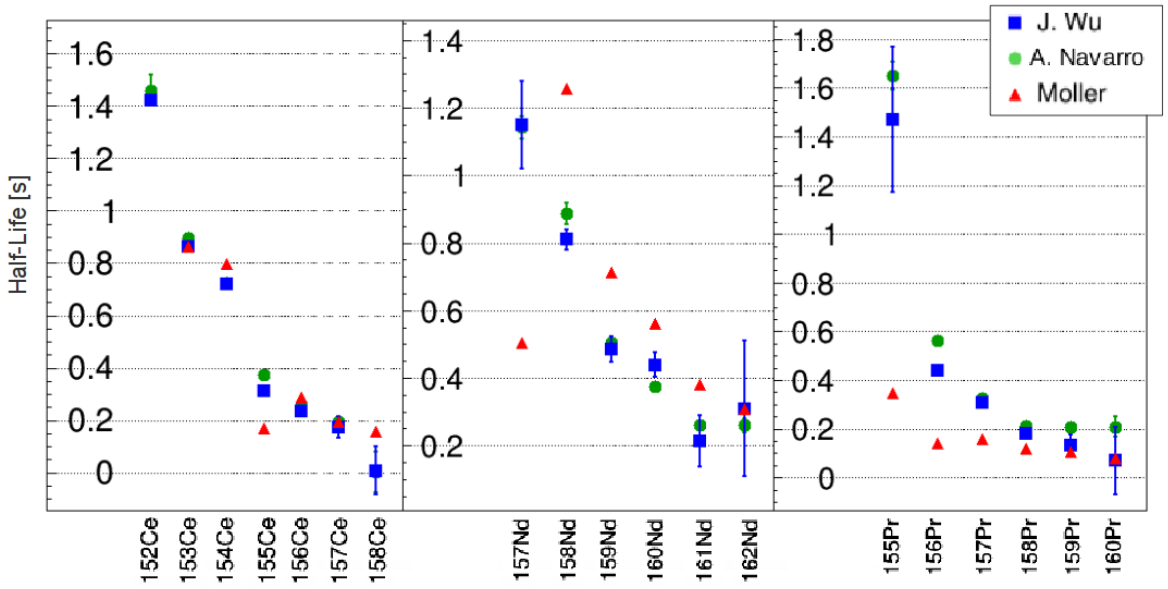

Figure 33: Systematic trends of β-decay half-lives from this work (green circles), compared with EURICA's campaign (Blue squares) [19] and Möller's theoretical predictions (Red triangle) [12]

We can clearly observe how the values obtained in the present analysis follow the experimental tendencies previously measured. A clear observable difference between the results calculated for this project and EURICA's experimental values, are the statistical uncertainties in half-life values. For BRIKEN's experiment, the mass spectrometer (BigRIPS) was optimized to obtain higher production rates for nuclei further away from stability line, as indicated in Subsection 1.5, Figure 6. This small difference in the settings subsequently pro-

duced differences in the production rates of the different nuclei. For less exotic nuclei (^{152}Ce, ^{156}Pr, $^{157-158}Nd$), the uncertainty obtained in this work was larger than the one obtained by EURICA's campaign. For more exotic nuclei the tendency is the opposite.

The results summarized in figure 33 serve as a prove of the success of NP1612-RIBF148's experiment. The analysis performed for the present work is only a preliminary analysis. A more detailed off-line analysis will be necessary in order to report proper half-life values and uncertainties. Even so, this preliminary analysis was indispensable to gain a clear understanding of the potential of October 2018's data. This analysis clearly shows the success of the experimental campaign and the great potential of the current available data.

6. Summary and Perspective.

The objective of the BRIKEN collaboration is to measure nuclear properties ($T_{1/2}$ and P_n) values of exotic nuclei contributing to the rapid neutron capture process. For this project, a preliminary data analysis of NP1612-RIBF148's experiment (October 2018 campaign) was performed. The objective of this preliminary analysis was to obtain the half-lives of the nuclei $^{152-158}Ce$, $^{155-160}Pr$ and $^{157-162}Nd$. These nuclei contribute greatly to the formation of the REP peak, an increase in the elemental solar abundances around mass A $\sim$ 160 (Section 1).

In order to perform this data analysis, first, a detailed understanding of the experimental set-up was necessary. The experiment was performed at RIBF RIKEN, exploiting the high-intensity ^{238}U beam from which the neutron-rich nuclei of interest were produced by in-flight fission. After it's production and separation in BigRIPS (Subsection 2.1) this nuclei are implanted into the highly segmented silicon stopper array, AIDA (Subsection 2.2). BRIKEN Neutron counter measured the β-delayed neutrons emitted during the decay of implanted nuclei (Subsection 2.3). For this project only half-lives were calculated, thus, no further mention about BRIKEN's data treatment was given. Each one of these systems has its own data acquisition system. For a proper data analysis attention has to be payed to the sorting of the data of each one of this DAQs separately. For this project the near-line data analysis of the merged data was performed. For this analysis a C++ software program was implemented.

The methodology behind this software program has been detailedly explained in section 4. October 2018's experiment used a total of 65h of beam time, from which 60h have been analyzed. The half-lives calculated for this report had already been measured by EURICA's campaign. This preliminary analysis yielded very promising results, that agreed to a great extent with previously measured values, as shown in subsection 5.3. Improvements in the statistical uncertainties were accomplished. The preliminary results shown in this report shows the great success of October 2018 campaign and serves as a starting point for the proper off line analysis.

One of the first steps for a proper off line analysis would be the cleaning of the PID plot obtained by BigRIPS. A first cleaning was already applied during October's experiment, but the clear presence of charge states makes the miss-identification of isotopes a major problem that needs to be worked on. At the moment two different sorting programs are available for sorting AIDA's data. For this project, LuckyDoll software was used. For a proper data analysis, the parameters needed for sorting AIDA's data should be optimized. All data should be reprocessed using the latest version of LukyDoll or Oscar Hall's program. This reprocessing of the data wold help reducing the uncorrelated β-implant background and it would eliminate the 20ms bump.

Very promising data is hiding behind the β-neutron-implant correlation histograms. BRIKEN's data for the experiment has to be reprocessed with the correct initial conditions. The implemented C++ software program is currently not able to calculate P_n values but it's modulated programming should make the addition of this feature not extremely complicated. A.Tosas article [44], detailedly explains the particularities of P_n values calculations. P_n values of nuclei in this region have never been measured thus it's calculation is crucial enhancing our knowledge of the REP peak formation process.

Appendix A:

Half-life calculation software. Detailed description and usage.

This analysis software was implemented using C++ and ROOT v6.10.08, Linux-ubuntu16.04 and gcc5.4. This program focuses on the analysis of the merged data after it has been processed with the AnaMerger software (See Sec 2.4 for more details about the data structure up to this point).

A.1 File Structure

For the program to be executed several files are necessary. Figure 34 is trying to represent visually the program's structure. One could classify the files in three categories, main files, input files and output files. Let's first focus on the main files (black square in figure 34). First of all, the file with the data to be analyzed is necessary. In Figure 34, this data file is named "ALL_MERGED_BRIKEN2018.root". This file corresponds to the merged file of all the runs of the experiment after being processed by the AnaMerger software program. This file contains the necessary 1D and 2D histograms for the data analysis.

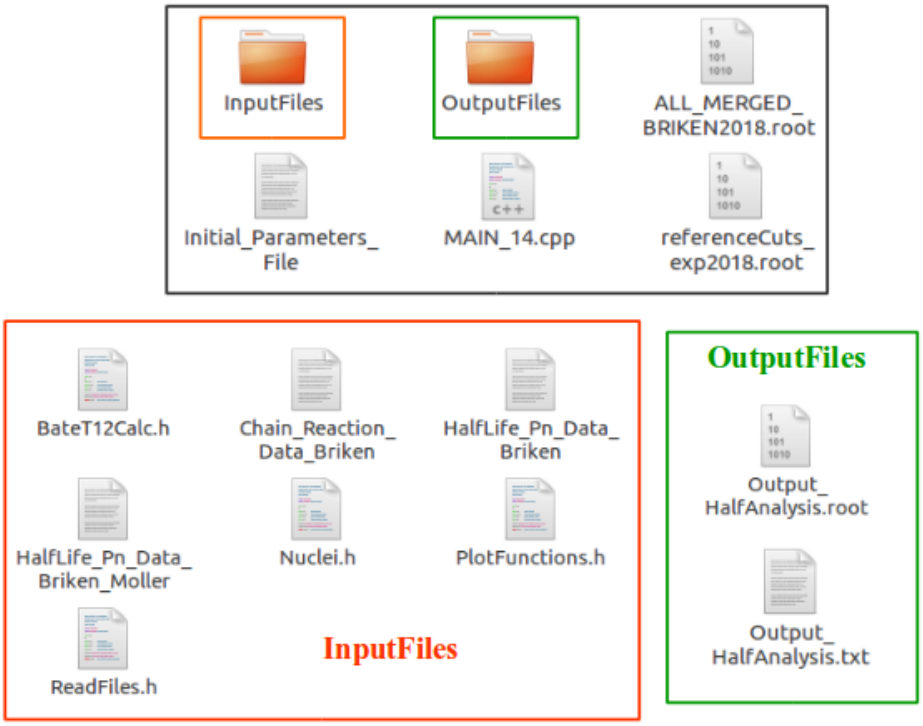

Figure 34: Files necessary for the half-life program to be executed.

The file "referenceCuts_exp2018.root" contains the cuts applied in the AnaMerger step for isotopic selection. Here this file is necessary for the β-efficiency calculation. The folder structure must remain as indicated in figure 34. If this structure is changed, the paths must be appropriately modified in "MAIN_14.cpp".

A.2. Main Program structure.

In order to execute the program the "MAIN_14.cpp" has to be loaded into roots environment. This main file first loads the libraries and secondary code files necessary for its execution. This main file contains only one function. This function needs as an input parameter the name of a file containing some of the necessary parameters for the analysis.

```
int FITTING_PROGRAM(std::string Ini_Par_File_Name)
```

The format of this input file must be the same as the one followed by the "Initial_Parameters_File" document. In figure 35 an example of input file has been represented. Once this function is executed, the program will proceed with the data analysis of the nuclei indicated in the input file.

```
-----------------------------------------
    Necessary Parameters for Analysis
-----------------------------------------

-> Name of the parent Isotope [252Cf]
Number of Nuclei:  7
155Pr
156Pr
157Pr
158Pr
159Pr
159Pr
160Pr
-> Calculo Valor T1/2 [0: No    1: Si]
1
-> Calculo Valor Pn [0: No     1: Si]
1
-> Opciones Backgrownd [0: Pol0 ]
0
-----------> Name Data File:
ALL_MERGED_BRIKEN2018.root
-----------> Cuts File Name:
referenceCuts_exp2018.root
-----------> Output Folder Name:
OutputFiles
```

Figure 35: Example of Input File format.

Nevertheless, before the half-life calculation starts, more file reading is necessary.

```
// Reads Initial Parameters File
std::tuple <vector<std::string>, int, int, int, std::string, std::string,
std::string > IniPar_Tuple = ReadInitialParFile(Ini_Par_File_Name);
```

```
// Reads Nuclei Information
    std::map<std::string, Nuclei * > M_NUCLEIS = ReadDataBase();
```

With the first instruction, the information in the Input File aforementioned (Figure 35) is uploaded. The second instruction proceeds to the reading of a database, constructed for

this program, that contains the information of all the nuclei necessary for this analysis. The functions "ReadInitialParFile()" and "ReadDataBase()", are defined in file "ReadFiles.h", that can be found inside InputFiles folder. Function "ReadDataBase()" needs two more files, Figures 36 and 37 show how this two files format must be. If other nuclei are necessary, they can be easily added by just including them in this files. The names of this two files must remain constant or be modified in file "ReadFiles.h".

```
-------------- Half Life Database -------------------
Si se añade un nuevo nucleo añadir tb en Number_of_Nuclei
Nuclei Z  A  T12 [s]  err_up_T12[s]  err_down_T12[s]  Pn Err_up_Pn  Err_down_Pn
-------------------------------------------------------------------------------
Number_of_Nuclei 68
150Ce   58      150     6.05    0.07    0.07    0       0.2     0
151Ce   58      151     1.76    0.06    0.06    0       0.2     0
152Ce   58      152     1.42    0.02    0.02    0       0.2     0
153Ce   58      153     0.865   0.0025  0.0025  0.0002  0.2     0
154Ce   58      154     0.722   0.0014  0.0014  0.0011  0.2     0
```

Figure 36: Part of the file containing the information about the properties of the different nuclei that might be involved in the analysis.

```
------------- Chain Reaction Database ---------------
Primero Todos los que decaen por beta decay, luego los neutron y bta decay.
Parent Daughter Grand-Daughter Neutron-Parent Neutron-Daughter ...
-----------------------------------------------------------------
Number_of_Chains    32    Number_of_Decays    4
150Ce    150Pr   150Nd   149Pr   149Nd
151Ce    151Pr   151Nd   150Pr   150Nd
152Ce    152Pr   152Nd   151Pr   151Nd
153Ce    153Pr   153Nd   152Pr   152Nd
154Ce    154Pr   154Nd   153Pr   153Nd
```

Figure 37: Part of the file containing the information about the decay chains of the different nuclei that might be involved in the analysis

After reading this files, the MAIN program proceeds to upload both, the cuts file ("reference-Cuts_exp2018.root") and the data file ("ALL_MERGED_BRIKEN2018.root"). This files are .root files and contain the necessary cuts for nuclei identification, and the decay histograms needed for the analysis respectively. The naming format of this TCutG, TH1D and TH2D objects must follow the same naming code as in this two files or be modified in "MAIN_14.cpp".

Once this file reading step is fulfilled, the program creates two empty files in the "OutputFiles" folder. This two files will contain the results of this analysis program. If this files were already existent in the folder, they will be erased and created again. An independent analysis is executed for each one of the nuclei indicated in "Initial_Parameters_File", but the results of all this nuclei will be available in this two output files.

```
1    // Creates Output Folder and Output Files
2  std::string Output_Folder_Name = std::get<6>(IniPar_Tuple);
3  std::string  order_delete_directory = "rm -rf "+Output_Folder_Name;
4  system(order_delete_directory.c_str());
5  std::string order_create_directory = "mkdir "+Output_Folder_Name;
6  system(order_create_directory.c_str());
7
8  TFile*Output_root_file = TFile::Open("Output_HalfAnalysis.root","RECREATE");
9  std::ofstream Output_txt_file("Output_HalfAnalysis.txt");
```

Once all the preparations have been completed, the main program calls the analysis function.

```
    // ------------------------ CALCULATION T12 ----------------
    //    Inputs:
    //        Implant Beta correlation histogram
    //        Background Option -> 0: Flat Background
    //        Map with all the nuclei information
    //    Output:  vector<double>
    //        0: X0 Value, Activiti Binwidth
    //        1: Half Life From analysis [s]
    //        2: Error Half life analysis [s]
    //        3: VAlue Of the Background
    //        4: Beta Efficiency Value
    //        5: Error of the beta efficiency value
    //        6: Background sigma
    //        7: X0 sigma
    // ---------------------------------------------------------

V_t12_from_Analysis = T12_Calculation(Imp_Bta_Histo, cuts_file, root_file,
   Output_root_file, std::get<3>(IniPar_Tuple), M_NUCLEIS);
```

The analysis function "T12_Calculation(...)" is defined in "BateT12Calc.h" alongside with other functions necessary for its execution. In the following section a detailed description of "T12_Calculation(...)" can be found. Ther is one more file that has not been tackled up to now. This is the "Nuclei.h" file. This file is necessary because of how the definition of nuclei is implemented into the program. In this program, each nuclei is an object of the class Nuclei, a user defined data type. The "Nuclei.h" file holds the information about data members and member functions, which can be accessed and used by creating an instance of that class, a Nuclei object.

A.3 Analysis Program Structure.

This function begins by calculating the background of the TH1D implantβ histogram. The type of function used for the background determination is indicated in the "Initial_Parameters_File" document. Currently, the only option implemented is the fat background option, but othe options could be easily implemented by adding more conditions in this if, else statement.

```
    if (Op_Backgrownd == 0){
     ib_histo->Fit("pol0","Lq0","0",firstbin,0);
     VAl_Backg = ib_histo->GetFunction("pol0")->GetParameter(0);
     Err_Backg = ib_histo->GetFunction("pol0")->GetParError(0);
     }
```

Following the background determination, the program generates the fitting function for the implant-β histogram. This function is detailedly explained in section 3.1.

```
    TF1 * Fit_t12 = new TF1("myfunc", BateFunc, bw, lastbin, 10);
```

"BateFunct" contains the detailed description of the function and it is defined in this "BateT12Calc.h" file. This function depends on some parameters as indicated in section 3.1. All these parameters are going to be introduced into the program as random Gaussian variables.

```
    // Random number generator initialization.
  TRandom3 *RDM  = new TRandom3(); RDM->SetSeed(0);
```

The program is then executed a thousand times. The number of times it is executed can be easily changed by modifying the variable "Nrolls". For each one of this executions, first an educated guess is given to the half life and initial activity of the parent nuclei. Nuclei with very low statistics implant-β statistics can be very sensitive to this initial guess. Afterwards, each one of the parameters needed by "BateFunct" function is generated randomly from a gaussian distribution with mean and sigma as the values indicated in $T12$ and err_up_T12" parameters in the "HalfLife_Pn_Data_Briken" file.

```
    // Initial guess for T12 and X0 of parent nuclei.
    Fit_t12->SetParameter(0, X00);
    Fit_t12->SetParameter(1, Parent->getT12()[0]);
    // Value of the other parameters.
    double r_t12_d  = ( RDM->Gaus(Daugh->getT12()[0],Daugh->getT12()[1]));
    double r_t12_gd  = ( RDM->Gaus(GDaugh->getT12()[0],GDaugh->getT12()[1]));
    double r_t12_nd  = ( RDM->Gaus(NDaugh->getT12()[0],NDaugh->getT12()[1]));
    double r_t12_ngd =(RDM->Gaus(NGDaugh->getT12()[0],NGDaugh->getT12()[1]));
    double r_Back  = ( RDM->Gaus( VAl_Backg , Err_Backg ) );
    double r_Pn_p  = ( RDM->Gaus( Parent->getPN()[0], Parent->getPN()[1]));
    double r_Pn_d  = ( RDM->Gaus( Daugh->getPN()[0], Daugh->getPN()[1]));
    double r_Pn_nd  = ( RDM->Gaus( NDaugh->getPN()[0], NDaugh->getPN()[1]));
     // ---- Let's fix the fit parameters --- //
    Fit_t12->FixParameter(2, r_t12_d);
    Fit_t12->FixParameter(3, r_t12_gd);
    Fit_t12->FixParameter(4, r_t12_nd);
    Fit_t12->FixParameter(5, r_t12_ngd);
    Fit_t12->FixParameter(6, r_Pn_p);
    Fit_t12->FixParameter(7, r_Pn_d);
    Fit_t12->FixParameter(8, r_Pn_nd);
    Fit_t12->FixParameter(9, r_Back);
```

Once all the parameters have been correctly uploaded in "BateFunct", the fitting of the experimental function can occur.

```
    // ---- And this is where magic happens --- //
    ib_histo->Fit("myfunc", "LR+0q", "", bw, lastbin);
```

From the "Fit_t12" function we can now obtain the values of the half-life and initial activity of the parent nuclei that better adjust the experimental decay curve, according to the Maximum Likelihood method. These values, as well as the random values for each one of the previous variables are then introduced into histograms that will help us obtain the final values of the half life and initial activity of the parent nuclei, but they will also serve as monitor the values of the initial parameters on the different executions.

```
    // ------------ Let's fill up the necessary histograms. ------- //
    {
    Parent->H1D_T12p->Fill(t12_fit);
    Parent->H1D_X0p->Fill(X0_fit);
    Parent->H1D_rT12d->Fill(r_t12_d);
    Parent->H1D_rT12gd->Fill(r_t12_gd);
    Parent->H1D_rT12nd->Fill(r_t12_nd);
    Parent->H1D_rT12ngd->Fill(r_t12_ngd);
    Parent->H1D_rPNp->Fill(r_Pn_p);
    Parent->H1D_rPNd->Fill(r_Pn_d);
    Parent->H1D_rPNnd->Fill(r_Pn_nd);
    Parent->H1D_rBack->Fill(r_Back);
    }
```

Once all the executions have been completed, the program procedes to the calculation of the final values for the half life and initial activity of the parent nuclei. $T_{1/2}$ and X_0

are calculated by fitting the previously filled histograms to a Gaussian function and taking the mean value of this Gaussian. The error of this two parameters takes into account three contributions. The main contribution is calculated as the sigma of this Gaussian variable, but the errors when calculating the mean and the sigma are also taken into account.

```
1  double mean_t12 = Parent->H1D_T12p->GetMean();
2  double mean_X0 = Parent->H1D_X0p->GetMean();
3  double t12_sigma = Parent->H1D_T12p->GetStdDev();
4  double X0_sigma = Parent->H1D_X0p->GetStdDev();
5
6  double t12_er = Parent->H1D_T12p->GetMeanError();
7  double sigma_err = Parent->H1D_T12p->GetStdDevError();
8  double X0_er = Parent->H1D_X0p->GetMeanError();
9  double X0_sigma_err = Parent->H1D_X0p->GetStdDevError();
10
11 double t12_sigma_fit = std::sqrt(t12_sigma*t12_sigma + t12_er*t12_er +
     sigma_err*sigma_err);
```

The only calculation remaining is the determination of the β-efficiency. For this calculation, the TH2D histogram containing the PID plot is uploaded. First, the number of implants measured by AIDA is calculated by integrating this PID plot conditioned to the appropriate cut. Afterwards the the number of implants is calculated by using the X_0 parameter just calculated. The error for this parameter is claculated in a simmilar manner to the previous one.

```
1
2  double N_implants = Nuc_Cut->IntegralHist(hImpl);
3
4  double mean_bta = mean_X0/( N_implants * ib_histo->GetXaxis()->GetBinWidth(0)
     );
5  double sigma_bta = std::sqrt(X0_sigma*X0_sigma + X0_er*X0_er + X0_sigma_err*
     X0_sigma_err)/( N_implants * ib_histo->GetXaxis()->GetBinWidth(0));
```

A.4 Output Files and Results.

Once the values of the half lives and initial activities have been calculated for all the nuclei indicated in "Initial_Parameters_File", the output files are written and created. Figures 38 and 39 show the content of "Output_HalfAnalysis.root" and "Output_HalfAnalysis.txt" after executing the program with the input file in figure 35. "Output_HalfAnalysis.root" is a root file and contains the histograms generated during the program execution, such as the values of the different parameters used for the simulations, or the $T_{1/2}$ and X_0 histograms. "Output_HalfAnalysis.txt" contains a table with a summary of the results obtained during the simulations.

```
KEY: TCanvas  C_T12fit_155Pr;1
KEY: TH1D     H1D_X0p_156Pr;1
KEY: TH1D     H1D_T12p_156Pr;1
KEY: TH1D     H1D_rT12d_156Pr;1
KEY: TH1D     H1D_rT12gd_156Pr;1
KEY: TH1D     H1D_rT12nd_156Pr;1
KEY: TH1D     H1D_rT12ngd_156Pr;1
KEY: TH1D     H1D_rPNp_156Pr;1
KEY: TH1D     H1D_rPNd_156Pr;1
KEY: TH1D     H1D_rPNnd_156Pr;1
KEY: TH1D     H1D_rBack_156Pr;1
```

Figure 38: Example of content of "Output_HalfAnalysis.root" file.

```
Summary of the results from T12 and Pn calculations
                          Program: HalfLife_12
 Nuclei  |  Background |  Half Life [J. Wu] |  Half Life [Analysis] |  Beta Eff.
-------------------------------------------------------------------------------
 155Pr   2062.09+-2.0308      1.47+-0.3        1.6518+-0.059272     0.271631+-0.00866495
 156Pr   3814.87+-2.7622      0.444+-0.006     0.561969+-0.0127972  0.250967+-0.00437039
 157Pr   2879.57+-2.39982     0.307+-0.021     0.324261+-0.0200023  0.222607+-0.0125058
 158Pr   290.75+-0.762562     0.181+-0.014     0.210764+-0.00554329 0.212315+-0.00458541
 159Pr   65.162+-0.361004     0.134+-0.043     0.207149+-0.0112286  0.187909+-0.00819484
 160Pr   10.144+-0.142436     0.069+-0.14      0.208432+-0.0385169  0.15103+-0.0403171
```

Figure 39: Example of "Output_HalfAnalysis.txt" file

The program also executes several functions created for a visual representation purposes. This functions are defined in "PlotFunctions.h" file.

```
1 Plot_HalfLife_Fitting(Imp_Bta_Histo, Output_root_file, Nuclei_Name, M_NUCLEIS,
      V_t12_from_Analysis);
2 Plot_HalfLife_Comparison(Output_root_file, V_Nuclei_Names, M_NUCLEIS,
      V_t12_all_nuclei);
```

Plot_HalfLife_Fitting(...)" represents the implant-beta decay curve with the analytic model superimposed, such as in figure 32. "Plot_HalfLife_Comparison(...)" represents a pointlike graph comparing the previously obtained results with the ones found in literature, such as in figure 33.

References

[1] A. Eddington, *The internal constitution of stars*. The observatory. The monthly review of astronomy. October 1920.

[2] E.Margaret,et. al, *Synthesis of the Elements in Stars*. Synthesis of the Elements in Stars, Volume 29, Number 4 Ocrober, 1957.

[3] Michael S. Smith and K. Ernst Rehm. *Annual Review of Nuclear and Particle Science*. Vol. 51:91-130 (Volume publication date December 2001)

[4] Burbidge, E. M., Burbidge, G. R., Fowler, W. A., Hoyle, F. (1957). *Synthesis of the Elements in Stars*. Reviews of Modern Physics. 29 (4).

[5] R. Reifarth, et. al. *Neutron Reactions in Astrophysics*. Topical Review, 22 Mar 2014.

[6] M. Arnould, S. Goriely, and K. Takahashi, *The r-process of stellar nucleosynthesis: Astrophysics and nuclear physics achievements and mysteries* . Phys.Rept.450:97-213,2007

[7] D. Kasen, et. al. *Origin of Heavy elements in binary neutron star mergers from a gravitational wave event.* Nature, 16 Oct 2017.

[8] Krane, Kenneth S. *Introductory Nucleare Physics* . Wiley, New York, NY, 1988.

[9] Sabrina Strauss. *Beta-Delayed Neutron Emission Using the Beta Paul Trap*. University of Notre Dame. Stewardship Science Annual Review June 28, 2016

[10] M. R. Mumpower, et. al. *Reverse engineering nuclear properties from rare earth abundances in the r process*. 30 sep 2016. LA-UR-16-27225.

[11] M. R. Mumpower, et. al. *The impact of individual nuclear properties on r-process nucleosynthesis*. Progress in Particle and Nuclear Physics, 86:86–126, January 2016.

[12] P. Möller, et. al. *New calculations of gross -decay properties for astrophysical applications: Speeding-up the classical r process*. Phys. Rev. C, 67(5):055802, May 2003.

[13] T. Yoshida and T. Tachibana. *Theoretical Treatment of the Asymptotic Behavior of Fission Product Decay Heat toward Very Short Cooling-Time*. Journal of Nuclear Science and Technology, 37:491–497, June 2000.

[14] National Nuclear Data Center, Evaluated Nuclear Data File (ENDF).

[15] M. Vilén, et. al. *Precision mass measurements on neutron-rich rare-earth isotopes at JYFLTRAP reduced neutron pairing and implications for the r-process calculations*. Phys. Rev. Lett. 120, 262701 (2018)

[16] Xu Zhengyu. *Beta-decay spectroscopy on neutron-rich nuclei in a range of Z = 26 32*. PhD, Graduate School of the Faculty of Science, Dongjing University.

[17] M. R. Mumpower, et. al. *Formation Of The Rare Earth Peak: Gaining Insight Into Late-Time r-Process Dynamics*. Physical Review C 85(4) · September 2011.

[18] Ciccone, Stephanie, TRIUMF/McMaster University 2013.

[19] J. Wu, et al. *94 -Decay Half-Lives of Neutron-Rich 55 Cs to 67 Ho: Experimental Feedback and Evaluation of the r-Process Rare-Earth Peak Formation.* PRL 118, 072701 (2017)

[20] V. H. Phong et al. to be published

[21] O. Hall et al. to bepublished

[22] H. Koura, et. al. *Nuclidic Mass Formula on a Spherical Basis with an Improved Even-Odd Term* Prog. Theor. Phys. 113, 305 (2005).

[23] T. Marketin, et. al. *Large-scale evaluation of β-decay rates of r-process nuclei with the inclusion of first-forbidden transitions*, Phys. Rev. C 93, 025805 (2016).

[24] Melanie Hampel, *Neutron capture nucleosynthesis and the i process*, Master of Science (M.Sc.), Universität Bonn.

[25] J. L. Tain et al. Acta Physica Polonica B 49, 417-428 (2018).

[26] RIKEN Wako, Saitama-ken, Japan.

[27] A. Tarifeño-Saldivia, et. al. *Progress on the measurements of Pn-values and half-lives for understanding the formation of the r-process rare-earth peak.* RIKEN APR report 2019.

[28] J.L. Tain. *The BRIKEN project: extensive β-delayed neutron measurements for atrophysics. JINA-CEE Seminar, February 11, 2019*

[29] Formation of an accelerator complex to generate RI beam. RIKEN, Nishina Center, Webpage.

[30] Toshiyuki Kubo, et. al. *BigRIPS separator and ZeroDegree spectrometer at RIKEN RI beam factory.* Prog. Theor. Exp. Phys. 2012.

[31] N. Fukuda, et. al. *Identification and Separation of Radioactive Isotope Beams by the BigRIPS Separator at the RIKEN RI Beam Factory.* Nucl. Instrum. Meht. B 317, 323 (2013)

[32] K. Nakamura et al. *Passage of particles through matter.* February 16, 2012, JP G 37 075021.

[33] P.F.F.Carnelli, et. al. *Multi-Sampling Ionization Chamber (MUSIC) for measurements of fusion reactions with radioactive beams.* Volume 799, 1 November 2015

[34] A. Mapelli. *Scintillation Particle Detectors Based on Plastic Optical Fibres and Microfluidics.* PhD, EPFL 2011.

[35] H. Kumagai, et. al. *Development of Parallel Plate Avalanche Counter PPAC for BigRIPS fragment separator.* Manuscript accepted for publication in NIMB.

[36] C.J. Griffin, et. al. *β -decay studies of r-process nuclei using the Advanced Implantation Detector Array (AIDA).* XIII Nuclei in the Cosmos, July, 2014, December, Hungary.

[37] Alfredo Estrade. *Status of the Advanced Implantation Detector Array (AIDA).* BRIKEN Collaboration Workshop Valencia, July 2015.

[38] A. Tarifeno-Saldivia, et. al. *Conceptual design of a hybrid neutron-gamma detector for study of β-delayed neutrons at the RIB facility of RIKEN.* J. Instrum 12 (2017) P04006.

[39] A. Tarifeño-Saldivia, A. Navarro, F. Calviño, *BRIKEN-140H neutron efficiency.* Feb. 26, 2018 BRIKEN analysis meeting.

[40] W. Królas et al. *First observation of the drip line nuclei 140Dy: Identification of a 7 us K isomer populating the ground state band*, Phys. Rev. C 65 (202) 031303.

[41] Instituto de Técnicas Energéticas (INTE) de la Universidad Politécnica de Cataluña, Barcelona, Spain.

[42] Oak Ridge National Laboratory, Bethel Valley Rd, Oak Ridge, TN 37830, EE. UU.

[43] ROOT - An Object Oriented Data Analysis Framework.

[44] A. Tolosa-Delgado, et. al. *Commissioning of the BRIKEN detector for the measurement of very exotic β-delayed neutron emitters.* 2 August 2018.

[45] H. Bateman. "Solution of a System of Differential Equations Occurring in the Theory of Radio-active Transformations," Proc. Cambridge Phil. Soc. IS, 423 (1910)

[46] Vi Ho Phong. *Report on AIDA and, WAS3ABi sort.* Feb. 26, 2018 BRIKEN analysis meeting.

[47] Wu Jin, *Study on -decay of neutron-rich nucleus Nuclear charge number Z=55-67.* PhD, Peking University, Beijing, May, 2016, May

[48] Oscar Hall. *Analysing AIDA Data, From an AIDA Point of View.* Feb. 26, 2018 BRIKEN analysis meeting.

[49] http://lise.nscl.msu.edu/lise.html

[50] N. Fukuda, et. al, *Identification and Separation of Radioactive Isotope Beams by the BigRIPS Separator at the RIKEN RI Beam Factory.* Nuclear Instruments and Methods in Physics Research Section B, Volume 317, 15 December 2013.

[51] Wu Jin, Study on -decay of neutron-rich nucleus Nuclear charge number Z=55-67. PhD, Peking University, Beijing, May, 2016, May